High Temporal Resolution Analyses with *GOES-16* Atmospheric Motion Vectors of Mesovortex Rapid Intensification in Subtropical Cyclone Henri (2021)

RUSSELL L. ELSBERRY,[a,b] JOEL W. FELDMEIER,[b] HWAY-JEN CHEN,[b] AND CHRISTOPHER S. VELDEN[c]

[a] *Lyda Hill Institute for Human Resilience, University of Colorado Colorado Springs, Colorado Springs, Colorado*
[b] *Department of Meteorology, Naval Postgraduate School, Monterey, California*
[c] *Cooperative Institute for Meteorological Satellite Studies, University of Wisconsin–Madison, Madison, Wisconsin*

(Manuscript received 12 August 2022, in final form 8 March 2023, accepted 27 April 2023)

ABSTRACT: Four-dimensional COAMPS dynamic initialization (FCDI) analyses with high temporal and spatial resolution *GOES-16* atmospheric motion vectors (AMVs) are utilized to analyze the development and rapid intensification of a mesovortex about 150 km to the south of the center of the subtropical cyclone, Cyclone Henri (2021). During the period of the unusual Henri westward track along 30°N, the FCDI $z = 300$-m wind vector analyses demonstrate highly asymmetric wind fields and a horseshoe-shaped isotach maximum that is about 75 km from the center, which are characteristics more consistent with the definition of a subtropical cyclone than of a tropical cyclone. Furthermore, the Henri westward track and the vertical wind shear have characteristics resembling a Rossby wave breaking conceptual model. The *GOES-16* mesodomain AMVs allow the visualization of a series of outflow bursts in space and time in association with the southern mesovortex development and intensification. Then the FCDI analyses forced by those thousands of AMVs each 15 min depict the $z = 13\,910$-m wind field responses and the subsequent $z = 300$-m wind field adjustments in the southern mesovortex. A second northern outflow burst displaced to the southeast of the main Henri vortex also led to a strong low-level mesovortex. It was when the two outflow bursts joined to create an eastward radial outflow all along the line between them that the southern mesovortex reached maximum intensity and maximum size. In contrast to the numerical model predictions of intensification, outflow from the mesovortex directed over the main Henri vortex led to a decrease in intensity.

KEYWORDS: Subtropical cyclones; Satellite observations; Numerical analysis/modeling

1. Introduction

a. Background on new analyses and satellite datasets

Elsberry et al. (2020) had described the opportunities, and the challenges, of utilizing high spatial and temporal resolution atmospheric motion vectors (AMVs) from new-generation geostationary meteorological satellites such as *GOES-16* to provide the four-dimensional analyses of tropical cyclones (TCs) during rapid intensification (RI) events, which are here defined as 30 kt $(24\ \text{h})^{-1}$ (1 kt $\approx 0.51\ \text{m s}^{-1}$). Elsberry et al. (2020) had modified an earlier dynamic initialization technique of Elsberry et al. (2018) to better utilize special reprocessed *GOES-16* AMV datasets by the University of Wisconsin Cooperative Institute for Meteorological Satellite Studies (CIMSS) at 15-min intervals to analyze and forecast an RI event in Hurricane Irma (2017). In addition to the routine *GOES-16* full-disk multispectral image scan every 10 min and the contiguous United States scanning every 5 min, the mesoscale scan mode allows 1-min imaging that can be targeted to follow a TC center within a 10° latitude × 10° longitude domain (Stettner et al. 2019; Lewis et al. 2020). Using this 1-min imagery, CIMSS has developed automated algorithms to produce very high spatial resolution AMVs, which greatly enhance the AMV coverage to resolve the small scales of the flow fields associated with the TC and its near environment (Elsberry et al. 2020).

The data assimilation challenge is to ingest these extremely high spatial density AMVs each 15 min and retain their information to continuously monitor the evolution of the TC vortex structure and associated intensity changes. Elsberry et al. (2020) describe their four-dimensional Coupled Ocean Atmospheric Model Prediction System (COAMPS) dynamic initialization (FCDI) technique that is a straight-forward and efficient method for assimilating these high temporal (15 min) and spatial resolution AMVs. In dynamic initialization, the 15-min AMV dataset wind components are interpolated in space to the COAMPS model grid points at that time to define a three-dimensional wind difference (or increment) field. For the next 15 min until a new AMV dataset becomes available, the AMV increments times a nudging coefficient are linearly added in the model zonal and meridional wind equations each time step to nudge those model wind components toward the AMV wind components. The larger the nudging coefficient, the more rapidly the model wind components will be adjusted toward the AMV winds. The COAMPS-TC model utilized in this study is triply nested. The fixed outer domain 1 has 361 grid points east–west and 191 grid points north–south with a grid spacing of 36 km. Domain 2 (domain 3) has 367 (556) grid points east–west and 331 (556) grid points north–south with a grid spacing of 12 km (4 km). Consequently, the entire *GOES-16* mesoscan AMVs domain is contained within domain 3 of the FCDI analyses with a grid spacing of 4 km.

In addition to these fundamentals of the FCDI technique that allowed it to be capable of incorporating more than 10 000 AMVs every 15 min, Elsberry et al. (2020, section 2.1.3 and their appendix) introduced a near-surface wind field adjustment that acts as a constraint on the low-level center translation, and consequently on the distribution of deep

Corresponding author: Russell L. Elsberry, relsberr@uccs.edu

DOI: 10.1175/WAF-D-22-0148.1

convection. In this surface wind adjustment in the assimilation cycle, the domain is translated every 15 min along a target pathway that is simply a straight line from the T = 0-h position to the known T + 6-h warning position. Because this surface wind field adjustment results in the FCDI analysis center predicted to be within fix uncertainty relative to the next warning position, the next 6-h assimilation cycle then simply begins from the previous 6-h assimilation position. Consequently, no vortex relocation or introduction of a bogus vortex at the warning position is required as in a cold start, and the FCDI analysis in the next 6-h assimilation cycle begins smoothly with no immediate adjustments in the wind field or in the mass field.

In addition to the documentation of the new FCDI technique, Elsberry et al. (2020) analyzed at 15-min intervals and forecast an RI event in Hurricane Irma (2017). The distinguishing feature of the Irma intensification period was first an extreme RI period, an intermediate constant intensity period, and then a slower RI period. Only the COAMPS-TC forecast initiated from a FCDI analysis that included the 15-min *GOES-16* AMV dataset accurately predicted the timing and persistence of the constant intensity period, and then resumed the deepening of Irma at the correct time and with an accurate rate of deepening. It is also important to note that the 15-min FCDI analyses have the capability to accurately specify the environmental wind fields that were interacting with the Irma outflow. Specifically, the COAMPS τ + 24-h forecast then had a stronger outflow in all quadrants that established direct connections with the adjacent synoptic circulations to the northeast and to the northwest, which Elsberry et al. (2020) assert was a key factor in an accurate prediction of the Hurricane Irma RI event.

b. *Tropical Storm Henri as a mission objective for the TCRI field experiment*

The research objectives of the Office of Naval Research Tropical Cyclone Rapid Intensification (TCRI) project are to better understand, analyze, and predict RI events, and especially the environmental and storm conditions, timings, and magnitude of RI events following TC formation. During the 2021 Atlantic hurricane season, the TCRI project collaborated with the NOAA Hurricane Research Division Advancing Prediction of Hurricanes Experiment (APHEX) to collect in situ aircraft observations in support of the TCRI research objectives. The NOAA P-3 and Gulfstream-IV were the primary aircraft, but the Air Force Reserve aircraft provided important in situ observations in between the NOAA research aircraft missions.

A summary of the intensity forecasts from the regional numerical models and their consensus along with the statistical–dynamical intensity guidance available to the TCRI mission planners at 1200 UTC 20 August is shown in Fig. 1. Note that the COAMPS-TC version utilizing the NCEP global model initial conditions and lateral boundary conditions (CTCX, blue line), which is typically accurate guidance, was predicting an extreme RI event (55 kt in 18 h) beginning at 1200 UTC 21 August. The NCEP regional model (HMON, green dots and line) was predicting an intensification from 65 kt at 0600 UTC 21 August to 90 kt at 0000 UTC 22 August. As indicated by the National Hurricane Center best track (BEST) in Fig. 1, such an RI event did not occur.

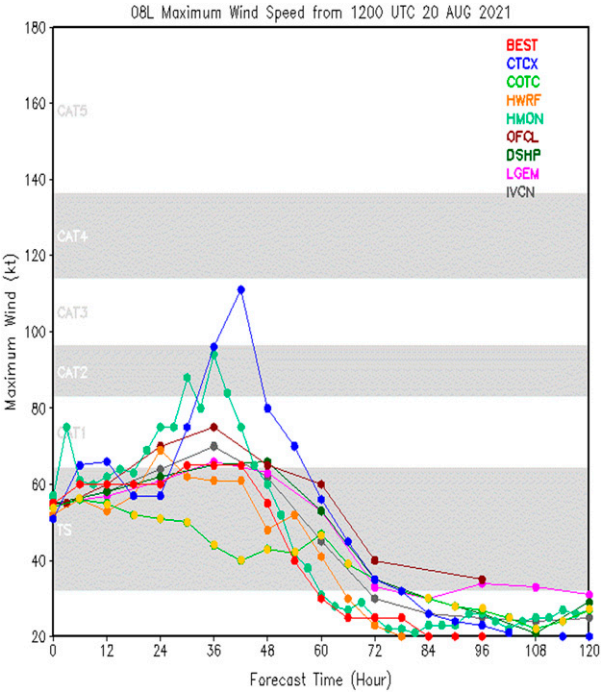

FIG. 1. Maximum wind speed (kt) forecasts from 1200 UTC 20 Aug for TS Henri by various regional numerical models (CTCX, COTC, HWRF, HMON), statistical–dynamic techniques (DSHP, LGEM), a consensus model (IVCN), and the NHC official forecast (OFCL) compared with the best track (BEST) intensity.

With this and other guidance, Tropical Storm (TS) Henri became a primary mission objective for the TCRI, and NOAA research aircraft missions were planned for Henri. Importantly for this study, NESDIS began targeting Henri with a *GOES-16* mesoscan sector that allowed CIMSS to provide high spatial and temporal (15 min) *GOES-16* AMVs beginning at 0915 UTC 20 August.

c. *Characteristics of the Henri RI life cycle*

Although Pasch et al. (2021) provide the official National Hurricane Center (NHC) report on Henri, the working best track (WBT) will be utilized here because that best corresponds with guidance products available in real time (Fig. 2). Henri started as a tropical depression at 1800 UTC 15 August near 34.1°N, 62.7°W and moved southward to become a TS at 1800 UTC 15 August near 31.1°N, 62.9°W. The two Henri phases of interest in this study are: 1) when strong Henri moved westward along 30°N; and 2) when around 0000 UTC 20 August Henri turned poleward and later accelerated toward the north-northeast. During the period from 0000 UTC 18 August to 0900 UTC 20 August, only routine hourly *GOES-16* AMV datasets were available. Then from 0915

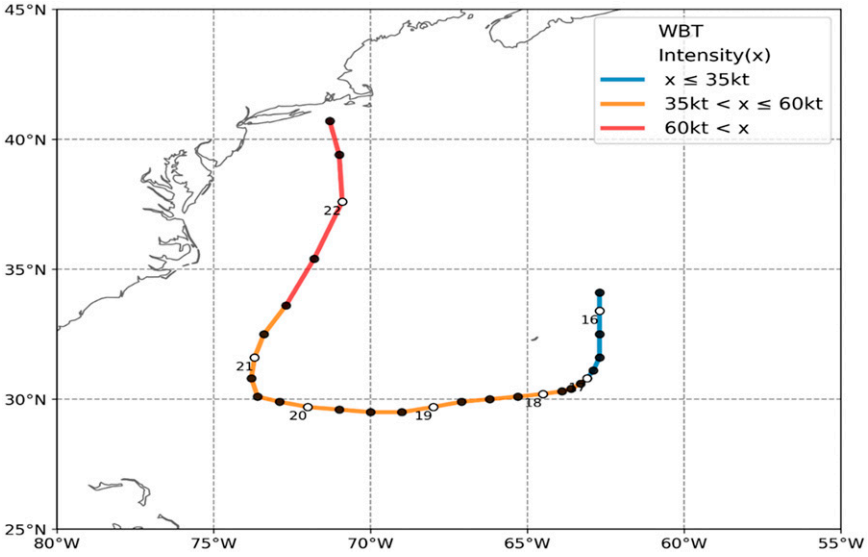

FIG. 2. Working best track (WBT, positions each 6 h) for the life cycle of Henri (2021). As indicated by the along-track line colors defined in the inset, Henri continued as a TS until 1200 UTC 21 Aug, and was then only a weak hurricane (65 kt) until 1200 UTC 22 Aug. It is noted that these WBT positions during 21–22 Aug differ somewhat from the NHC best track (Pasch et al. 2021, their Fig. 1).

UTC 20 August to 1415 UTC 21 August the 15-min *GOES-16* AMV datasets were available from CIMSS.

The intensity forecasts in Fig. 1 were initiated at 1200 UTC 20 August as TS Henri was turning poleward and crossing 30°W (Fig. 2). According to the initial intensities in Fig. 1, Henri was a strong TS (55 kt) and this TS intensity is indicated in Fig. 2 (inset) by an orange track segment, which according to the NHC WBT continued another 24 h until 1200 UTC 21 August when Henri became a hurricane. Whereas the CTCX had forecast an extreme RI event during the next 18 h (Fig. 1), according to the NHC WBT (Fig. 2) Henri did not further intensify beyond 65 kt during that 18-h period. It is noted that the COTC version of the COAMPS-TC that is initialized with the U.S. Navy global model (instead of the NCEP global model) forecasts a slow decay of the Henri vortex (Fig. 1, yellow dots along the green line). Since the COAMPS-TC model and vortex initialization are the same for COTC and CTCX, the explanation for these different intensity forecasts must be in the environmental conditions provided by the respective background global models. Following the Elsberry et al. (2018) conceptual model of the ocean cooling within the anticyclonic looping track of Hurricane Joaquin (2015), an early hypothesis for explaining the lack of a RI event as Henri moved poleward was due to strong ocean cooling to the right first along the westward path and especially during the slow turn poleward. Prompted by this hypothesis, the physical processes and vortex asymmetries along the westward path and during the slow poleward turn became another focus for the study.

There was large spread among the real-time intensity estimates upon which the NHC intensities were based (Fig. 3). After the two scatterometer observations (white crosses) around 1200 UTC 17 August, a large number of satellite-based intensity estimates were only between 32 and 45 kt when the best track (Fig. 3, black line) intensities at 1800 UTC 17 August to 0600 UTC 18 August were 55 kt. Although the satellite-based estimates after 0600 UTC 18 August were as large as 70–80 kt, the two high-quality scatterometer estimates around 0000 UTC 19 August were only 51–56 kt. Thus, the NHC analyst put the best track intensity at 60 kt from 1800 UTC 18 August to 1200 UTC 19 August before any in situ aircraft observations became available in Henri.

The first Air Force Reserve aircraft mission center fixes at 1730 and 1905 UTC 19 August were near 29.4°N, 71.0°W as Henri was about to begin the turn to the north (Fig. 2). As indicated in Table 1 (column 7), the average minimum surface pressure was 999 mb (1 mb = 1 hPa), which also agrees with the best track pressure in (Pasch et al. 2021, their Table 1). Note that the larger (48 kt) of the two maximum surface wind speeds (Table 1, column 6) is plotted at 1800 UTC 19 August in Fig. 3 (red triangles). However, the postseason best track intensity (black line) is 55 kt as the NHC analyst presumably relied more on the higher satellite intensity estimates.

The second Air Force mission center fixes straddled 1200 UTC 20 August, and the average of the maximum surface wind speeds was 39 kt (Table 1, column 6). Even though the aircraft-based intensities (red triangles) in Fig. 3 range from 32 to 48 kt, the best track intensity (black line) at 1200 UTC 20 August continued to be 55 kt, and was actually increased to 60 kt at 1800 UTC 20 August even though there were no satellite-based intensity estimates larger than 55 kt. The first two center fixes during the third Air Force Reserve mission were centered on 0000 UTC 21 August when Henri had translated poleward to near 31.4°N (Table 1, column 3). The maximum flight-level wind

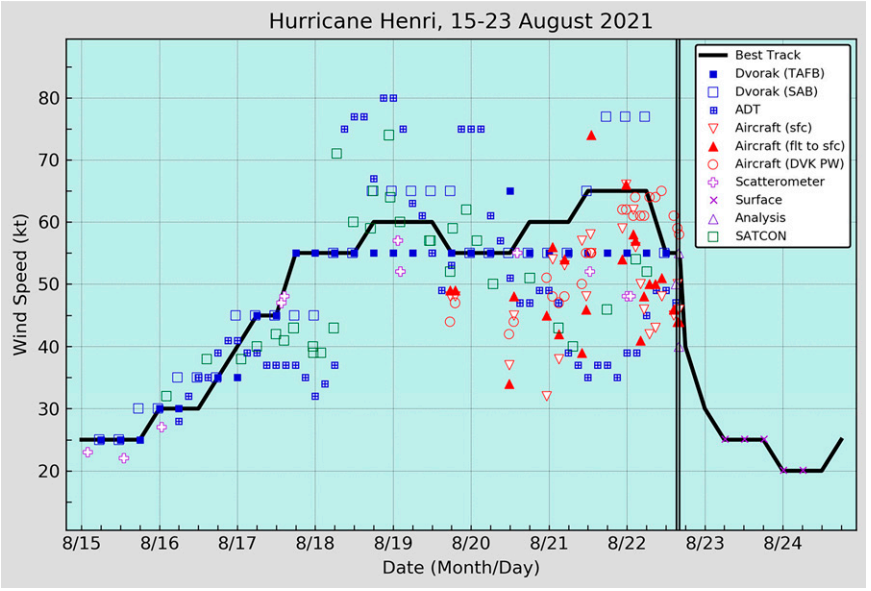

FIG. 3. Maximum wind speeds (kt; inset defines symbols) and the postseason NHC best track maximum surface wind speed (black line) for Henri (2021) during 15–23 Aug, with double vertical lines indicating landfall time. See Pasch et al. (2021) for further description.

speeds associated with these two fixes were 38 and 29 kt, but the maximum surface wind estimates were only 26 and 21 kt. However, these small surface wind estimates are not plotted in Fig. 3. Rather, two later surface wind estimates of 38 kt (adjusted to 43 kt) and 53 kt are included in Fig. 3, and again the best track intensity of 60 kt is not supported by any satellite-based intensity estimates above 55 kt at 0000 UTC 21 August.

The two center fixes during the fourth Air Force Reserve mission were centered on 1200 UTC 21 August when Henri had translated to near 33.4°N (Fig. 2). The two maximum surface wind estimates of 41 and 55 kt (Table 1, column 6) reflect some intensification, but not to the best track intensity of 65 kt at 1200 UTC 21 August. The maximum flight-level wind speed of 82 kt (Table 1, column 5) is presumably related to the aircraft wind of 75 kt (red triangle) at 1200 UTC 21 August in Fig. 3. A near-simultaneous *NOAA-42* aircraft mission reported a maximum flight-level wind of 65 kt (not shown), but it was noted that this flight-level wind was observed 71 n mi

TABLE 1. Maximum wind speeds (kt) associated with the Air Force Reserve aircraft center fixes in Henri (2021) taken from vortex messages. U1, U2, and U3 are code numbers for the three USAF Reserve aircraft flying that mission on that day.

	Fix information			Max wind (kt)		
Date of mission	Time (UTC)	Latitude	Longitude	Flight level	Surface	Pressure (mb)
19 Aug 2021 U1	1730	29.34°N	70.58°W	38	33	1000
	1905	29.58°N	71.09°W	61	48	998
20 Aug 2021 U2	1141	29.52°N	73.39°W	43	37	1000
	1308	30.05°N	73.25°W	60	41	1000
20 Aug 2021 U3	2314	31.28°N	73.55°W	38	26	995
	0102	31.45°N	73.37°W	29	21	997
	0259	32.02°N	73.36°W	52	38	998
	0445	32.03°N	73.27°W	67	53	997
21 Aug 2021 U1	1125	33.31°N	72.34°W	32	41	993
	1300	33.50°N	72.12°W	82[a]	55	993
22 Aug 2021 U1	0516	39.08°N	70.58°W	47	40	989
	0658	39.40°N	71.04°W	51	38	987
	0846	40.01°N	71.11°W	63	??	987
	1039	40.28°N	71.17°W	64	42	986
22 Aug 2021 U2	1424	41.05°N	71.35°W	42	45	989
	1532	41.15°N	71.41°W	55	50	990
	1604	41.18°N	71.46°W	42	46	991

[a] It is assumed that this 82-kt wind was not at the center (see text).

(1 n mi = 1.852 km) to the southeast of the center. It is assumed that the Air Force Reserve observation of 82 kt (Table 1) also was not near the center, but may have been southeast of the center. If so, the only support for the 65 kt best track intensity late on 21 August appears to be from the satellite-based operational Dvorak estimates from the Satellite Analysis Branch (Fig. 3, blue hollow square). It will be demonstrated below that the FCDI analyses of the intensity of the main Henri vortex was likely closer to the intensity from the fourth Air Force Reserve mission than from the satellite-based estimates depicted in Fig. 3. The fifth and sixth Air Force Reserve missions were during the period when Henri was rapidly translating toward a landfall in Rhode Island (Fig. 2), which is not a focus of this rapid intensification study.

While it is not normal practice to question the NHC best track intensity values, the first purpose of the above detailed discussion of the Air Force Reserve in situ intensity observations was to provide evidence that Henri may have been less intense during its westward path. The second purpose in documenting the Henri center fixes from 1200 UTC 20 August to 1200 UTC 21 August was that they provide supporting evidence that the main Henri vortex not only did not rapidly intensify during that time period, it likely decreased in intensity in association with an intense mesovortex to its south.

d. *Discovery of a rapidly intensifying mesovortex with a critical impact on TS Henri*

Instead of the focus being on that main Henri vortex, the development and rapid intensification of a separate mesovortex about 150 km to the south of the Henri main vortex is diagnosed with a continuous (15-min interval) set of FCDI analyses forced with *GOES-16* enhanced AMVs. The discovery of this Henri mesoscale vortex was after we had applied the FCDI analysis technique described in section 1a beginning from 0000 UTC 18 August (T = 0 h). The FCDI wind vector analyses at z = 300 and z = 13 900 m at 0600 UTC 21 August (T + 78 h) are shown in Fig. 4 (left column). While there was a cold-start initialization of the COAMPS component of the FCDI (Elsberry et al. 2020, Fig. 3), this T + 78-h analysis is then after 12 subsequent 6-hourly "warm starts." That is, each 6 h the lateral boundary conditions on domain 1 of the COAMPS were updated from the global model and the target 6-h center positions for the surface wind adjustment were updated. No other information about the main Henri vortex from the TC vitals (e.g., intensity or the radial wind structure) were utilized. For this first demonstration of the FCDI analyses of the Henri mesoscale vortex, no updates of the operationally available sea surface temperature (SST) analyses were made. Therefore, the T = 0-h SST analysis was retained throughout the continuous FCDI analysis period. Thus, the only environmental forcing from direct observations was the hourly *GOES-16* AMV datasets from 0000 UTC 18 August to 0900 UTC 20 August (T + 57 h), and then also 15-min *GOES-16* enhanced AMV datasets after 0915 UTC 20 August. The integration of the COAMPS model component of the FCDI with the AMV datasets and with the constraint of the surface wind adjustment for the positions creates the three-dimensional fields of the wind, mass, pressure, and humidity every 15 min.

The FCDI 300-m wind vector analysis in Fig. 4 has diagnosed an extensive area of strong low-level convergence relative to the mesovortex near 30.9°N, 73.4°W, and the associated isotach maximum is >30 m s^{-1}. By contrast, the center of the main Henri vortex near 32.4°N, 73.5°W is diagnosed as an oblong isotach minimum region, which is 1.5° latitude to the north of the mesovortex. As indicated in the top-left panel of Fig. 4, a radial outflow burst with the strongest outflow within the eastern semicircle is diagnosed at z = 13 910 m directly above the 300-m mesovortex center. Notice that the mesovortex outflow toward the north and the northwest terminates (isotach < 3 m s^{-1}) along 32°N, which is interpreted as a stagnation region in opposition with the southward outflow from the main Henri vortex. This stagnation region above the main Henri vortex is consistent with an arrested development of this vortex as suggested by the weaker maximum surface winds during the third Air Force Reserve mission (Table 1).

The Control COAMPS-TC initial wind vectors at z = 300 m and z = 13 910 m at 0600 UTC 21 August are shown in Fig. 4 (right column). In this Elsberry et al. (2020) version of the COAMPS used in the FCDI, there is a bogus vortex at z = 300 m that is superposed on a steering flow. With an initial intensity of 60 kt at 0600 UTC 21 August (Fig. 3), the bogus vortex z = 300-m wind field is much broader than in the FCDI analysis in the left column. Note that there is no evidence of a mesovortex in these Control z = 300-m initial conditions. Furthermore, there is no evidence of an associated outflow burst in the Control z = 13 910-m initial conditions in the top-right panel of Fig. 4. Rather, there is a minimum of wind speed near 30°N, 75.5°W (to the west-southwest of the mesovortex position near 30.9°N, 73.4°W), and there is a uniform south-southwesterly flow > 9 m s^{-1} directly over the main Henri vortex. The key point is the outflow burst associated with the Henri mesovortex is only resolved with FCDI analyses derived with the high spatiotemporal resolution *GOES-16* AMVs.

e. *Objectives of this study*

The primary objective of this study is to create a high temporal (15-min) validation dataset of these FCDI analyses with the *GOES-16* AMVs that can be utilized to analyze and predict the development and rapid intensification of the mesovortex in subtropical Henri. As a first step, the continuous FCDI analyses during the unusual westward track of Henri (Fig. 2) will be examined to determine how atmospheric environmental factors may have contributed to the mesovortex development. In a second step, the continuous FCDI analyses during and following the Henri poleward turn (Fig. 2) will be utilized to describe the early stage development and rapid intensification of the mesovortex, and then how the mesovortex blended into a north–south isotach maximum to the southeast of the main vortex. An integral aspect of that analysis will be the corresponding changes in the main Henri vortex during the life cycle of the mesovortex. Although in principle these FCDI analyses could be examined in 15-min intervals, less

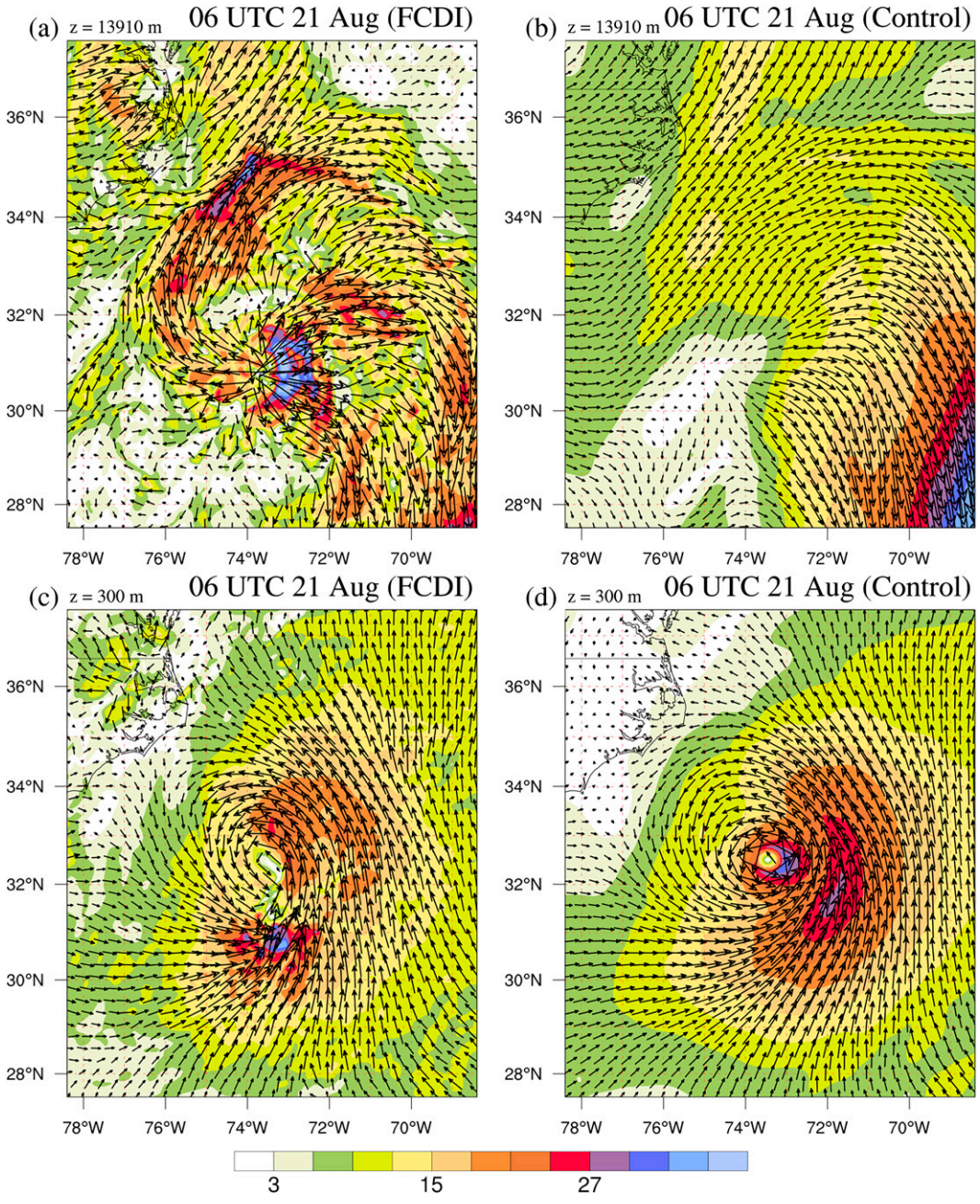

FIG. 4. Wind vectors (m s^{-1}; isotach color scale at bottom) at 0600 UTC 21 Aug (T + 78 h) (a),(c) from continuous FCDI analyses vs (b),(d) from the corresponding Control COAMPS initial conditions (bottom) at z = 300 m and (top) at z = 13 910 m.

frequent intervals (2–3 h) will be presented in consideration of publication limitations.

2. Continuous FCDI analyses of the environmental preconditions for the mesovortex development

Pasch et al. (2021) label Henri as an "unusual" storm. Although the early stages of Henri were in the subtropics, Pasch et al. (2021) do not label Henri as a subtropical cyclone, which in the NHC Glossary is defined as "*a non-frontal low pressure system that has characteristics of both tropical and extratropical cyclones. Like tropical cyclones, … have a closed surface wind circulation about a well-defined center …, often being associated with an upper-level low or trough.*" Unfortunately, the first *NOAA-49* (Gulfstream-IV) synoptic survey mission, which would have provided these upper-tropospheric observations, was not until 1748 UTC 19 August–0218 UTC 20 August when Henri was beginning its turn poleward.

TABLE 2. CIMSS vertical wind shear (VWS-C) magnitude and direction (360° is from north) estimates for Henri (2021) relative to the NHC TC Vitals positions from 0000 UTC 18 Aug to 0600 UTC 20 Aug, which is just prior to when the high temporal and spatial resolution *GOES-16* AMVs became available.

	NHC position		NHC intensity		VWS-C	
Date and time	Latitude	Longitude	Vmax (kt)	MSLP (mb)	Magnitude (kt)	Direction (°)
0000 UTC 18 Aug	30.23°N	64.27°W	55	994	5.8	297
0600 UTC 18 Aug	29.50°N	65.43°W	55	994	13.8	005
1200 UTC 18 Aug	30.03°N	66.14°W	55	994	16.0	021
1800 UTC 18 Aug	29.58°N	67.13°W	60	994	18.0	023
0000 UTC 19 Aug	29.53°N	68.15°W	60	991	27.3	034
0600 UTC 19 Aug	29.48°N	69.09°W	60	991	31.3	035
1200 UTC 19 Aug	29.30°N	70.09°W	60	991	31.5	044
1800 UTC 19 Aug	29.32°N	71.09°W	55	994	25.9	046
0000 UTC 20 Aug	29.51°N	71.56°W	55	994	20.2	034
0600 UTC 20 Aug	29.58°N	72.46°W	55	994	20.0	015

Wind analyses derived by CIMSS from the hourly *GOES-16* AMV datasets, and CIMSS deep-layer vertical wind shear (VWS-C) estimates (Table 2) during the westward path of Henri, provide evidence of a subtropical cyclone with an associated upper-troposphere trough. Except for the first (0000 UTC 18 August) VWS-C estimate, the magnitudes ramp up quickly to become well above the typical moderate value of 15 kt (Rios-Berrios and Torn 2017) with directions from out of the north at the beginning and changing to from the northeast at 1200–1800 UTC 19 August. Note that the largest VWS-C magnitudes of ~31 kt are at times when the NHC intensity estimates are the highest (60 kt), which is a counterintuitive correlation between VWS and TC intensity, but is consistent with the NHC definition of a subtropical cyclone.

The short-term (6 h) forecasts from the Control COAMPS-TC initial conditions during the westward path of Henri (Fig. 5) raise questions as to the vortex structure and intensity preconditions that existed before the mesovortex developed. As described with respect to the Control COAMPS-TC z = 300-m wind analyses in Fig. 4, the COAMPS-TC had a bogus vortex that was tied to the WBT TC Vitals as in Table 2. Thus, each 6-h track forecast (Fig. 5, top panel) started at the fix position, and during the westward path the first 6-h track forecasts were quite close to the next 6-h fix position. Note that it was at the end of the Henri westward track at 0600 UTC 20 August near 30°N, 72.5°W that the Control COAMPS-TC 6-h track forecasts first began to deviate to the east. By contrast, the continuous warm-start FCDI first 6-h track forecasts, which include the Elsberry et al. (2020) surface wind adjustment procedure with the target pathway being the next 6-h WBT position, are very accurate all along the westward Henri track.

Whereas the corresponding Control COAMPS-TC initial intensities (Fig. 5, bottom panel, red and gold lines) started at the WBT intensity (here m s^{-1} versus kt in Table 2), in every 6-h forecast along the westward path there was an instantaneous decrease of about 5 m s^{-1}, and a simultaneous increase in mean sea level pressure (not shown). This pattern of an instantaneous decrease followed by near-constant intensities until the next 6-h Control COAMPS-TC initial time continued until the 0600 UTC 20 August (end of Henri westward track) when a reintensification began to be noted within the first 6-h forecast period (see Fig. 4, right column for Control COAMPS-TC initial conditions). The CTCX intensity forecast (Fig. 1, blue line) from 1200 UTC 20 August is comparable to the next Control 6-h intensity forecast in Fig. 5 that has a peak intensity of 45 m s^{-1}

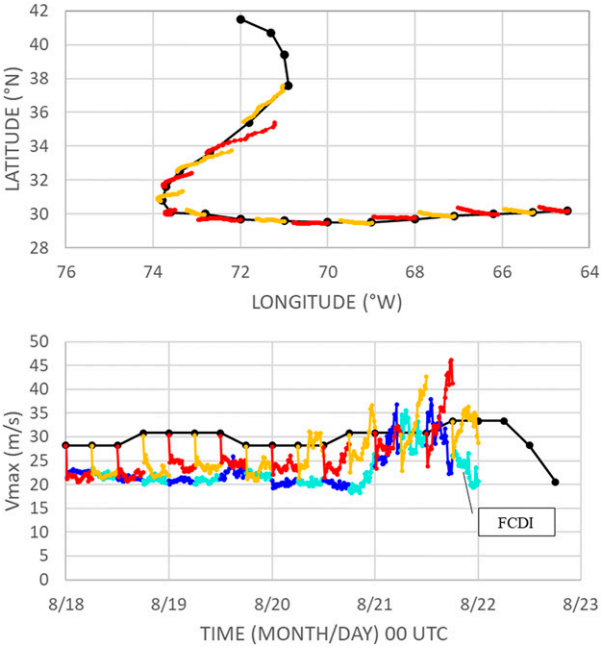

FIG. 5. (top) COAMPS-TC 6-h forecasts of Henri latitude and longitudinal track segments for the Control (alternating red and gold lines) starting from the NHC TC Vitals (black dots) every 6 h from 0000 UTC 18 Aug to 1800 UTC 21 Aug. Line colors are rotated from red to gold every 6 h to make it easier to visualize times of the forecasts. (bottom) Corresponding 6-hourly V_{max} (m s^{-1}) forecasts for the Control (alternating red and gold lines) and from the continuous warm-start FCDI analyses (alternating blue and aqua lines). Note the instantaneous V_{max} decreases of ~5 m s^{-1} at beginning of each 6-h intensity forecast for the Control, but only for the first FCDI analysis.

(red line labeled as Control). Because the continuous FCDI analyses also have a COAMPS cold start for the initial time of 0000 UTC 18 August, the same instantaneous decrease of about 5 m s^{-1} occurred as in the Control COAMPS Fig. 5 (bottom panel, blue lines). However, then the continuous FCDI analysis warm starts continued with Henri intensities more than 5 m s^{-1} lower than the WBT TC Vitals.

Whether it is the Control COAMPS-TC forecasts that are initialized each 6 h, or the continuous warm-start FCDI analyses that are forced with only hourly *GOES-16* AMVs during the Henri westward path, the interpretation is that Henri was a subtropical cyclone with an intensity of ~20–25 m s^{-1} (40–50 kt) rather than a tropical storm of 55–60 kt as in Table 2. While the NHC hurricane specialist had available some satellite fixes (Fig. 3) to support those NHC best track intensities, there are also Air Force Reserve aircraft fixes (Table 1) from 1800 UTC 19 August to 1200 UTC 21 August that support a weaker storm interpretation.

The 300-m vortex and 13 910-m environmental wind fields from the continuous FCDI analyses during the Henri westward track are provided at 1800 UTC 18 August (day 0.75) and at 0600 UTC 19 August (day 1.25) in Fig. 6, and then are continued at 1800 UTC 19 August (day 1.75) and 0600 UTC 20 August (day 2.25) in Fig. 7. Beginning with the z = 300-m wind analyses in Figs. 6c and 6d, note the highly asymmetric wind fields with near-zero wind speeds about 150 km to the southwest of the center, and 15 m s^{-1} winds extending more than 300 km to the north-northeast of the center. While the horseshoe-shaped isotach maximum is >21 m s^{-1}, it is about 75 km from the center. These two characteristics are consistent with the NHC definition of a subtropical cyclone: "*a radius of maximum winds occurring relatively far from the center (usually greater than 60 n mi), and generally have a less symmetric wind field*." While the FCDI z = 300-m wind analysis is becoming more symmetric with an isotach maximum > 24 m s^{-1} at 1800 UTC 19 August (Fig. 7c), the radius of maximum winds (Rmax) is about 60 km from the center. In the 0600 UTC 20 August z = 300-m wind analysis (Fig. 7d), the wind field is more symmetric, the isotach maximum extends well to the south, and even with the Rmax ~ 55 km to the north. Therefore, Henri's low-level wind structure is beginning to more resemble a TC than a subtropical cyclone.

In the z = 13 910-m wind field at 1800 UTC 18 August (Fig. 6a), there is not a clear outflow directly over the low-level center near 30°N, 67°W. Rather, there is a triangular area of light winds (<3 m s^{-1}) that is considered to be the residual of prior convective towers. Henri is advancing westward into a region with a broad jet (>25 m s^{-1}) extending to the southwest. Note that there is flow from the north that is being deflected to the southeast, which prevents it from getting to the center of Henri. Just 12 h later (Fig. 6b), Henri is now almost under the southwestward flow to the west, and the strengthened northerly flow has also encroached upon a small outflow region above and to the west of the Henri low-level center in Fig. 6d. This is the time (0600 UTC 19 August) when the VWS-C in Table 2 is 31.3 kt from 35° (i.e., from the northeast), which is consistent with these strong z = 13 910 wind flows near the Henri center, and the apparent vortex tilt of the outflow maximum relative to the low-level center.

Just 12 h later (Fig. 7a), the region of strong northerly winds in the northeast corner of Domain 3 in Fig. 6b has translated to the east while the Henri vortex at z = 300 m has continued translating westward to near 29.9°N, 71°W (Fig. 7c). A double outflow burst is diagnosed in Fig. 7a with a northern burst > 27 m s^{-1}, which is almost directly over the Henri z = 300-m vortex center. While an outflow burst in a weak environmental flow would be almost symmetrical, this Henri outflow burst is opposing the environmental northeasterlies to create a stagnation zone to the north-northeast of that Henri vortex position. The second, southwestern outflow burst isotach maximum is spread over a larger area, is stronger, and appears to have weakened and displaced the southwestward jet streak region that was present to the west of Henri just 12 h earlier (Fig. 6b). At 0600 UTC 20 August (Fig. 7d), the Henri z = 300-m vortex near 30°N, 72.9°W has weakened, but has become broader, especially to the west. A new region of low-level convergence is diagnosed near 29°N, 73.1°W where that broader vortex flow has merged with an isotach maximum band more than 100 km to the south of the center. Note also that the single radial outflow burst at z = 13 910 m (Fig. 7b) is almost directly over that region of low-level convergence, and the strongest outflow is directed to the south and to the southwest. Meanwhile, a region of upper-tropospheric flow from the northwest (Fig. 7b) has become superposed over the main Henri z = 300-m vortex (Fig. 7d), which is consistent with an arrested development of that main vortex.

These continuous FCDI analyses of events, which are primarily related to the upper-tropospheric environmental interactions with the Henri outflow as it moved westward, reveal the origin of a separate mesovortex. While these analyses are presented here at 12-h intervals. The FCDI analyses are available at hourly intervals for further study if necessary. However, the hourly AMVs do not resolve as well as the 15-min enhanced AMVs the details of the outflow bursts and their interaction with the environment (e.g., the outflow burst in Fig. 7b, and the upper-tropospheric flow extending over the Henri vortex).

Approximately 6 h after the FCDI analyses in Figs. 7b and 7d, the 15-min *GOES-16* AMVs became available, and the CIMSS AMV team has provided a special 15-min (VWS-C) plot within the *GOES-16* mesodomain at 1200 UTC 20 August (Fig. 8). Especially in the region of subtropical high pressure where the 850-mb winds are relatively light, these VWS-C vectors are dominated by the stronger 200-mb winds. For example, the region with VWS > 20 m s^{-1} (Fig. 8, white) in the southeast quadrant represents a strong upper-tropospheric trough. Although the VWSs to the north of Henri in Fig. 8 are not large, the VWS-C vectors indicate an anticyclonic flow (ridge) that extends well off the U.S. East Coast, and that ridge is considered to have been a dominant factor in the westward track of Henri. Note also the shortwave trough and ridge that are propagating eastward along the northern boundary of the ridge.

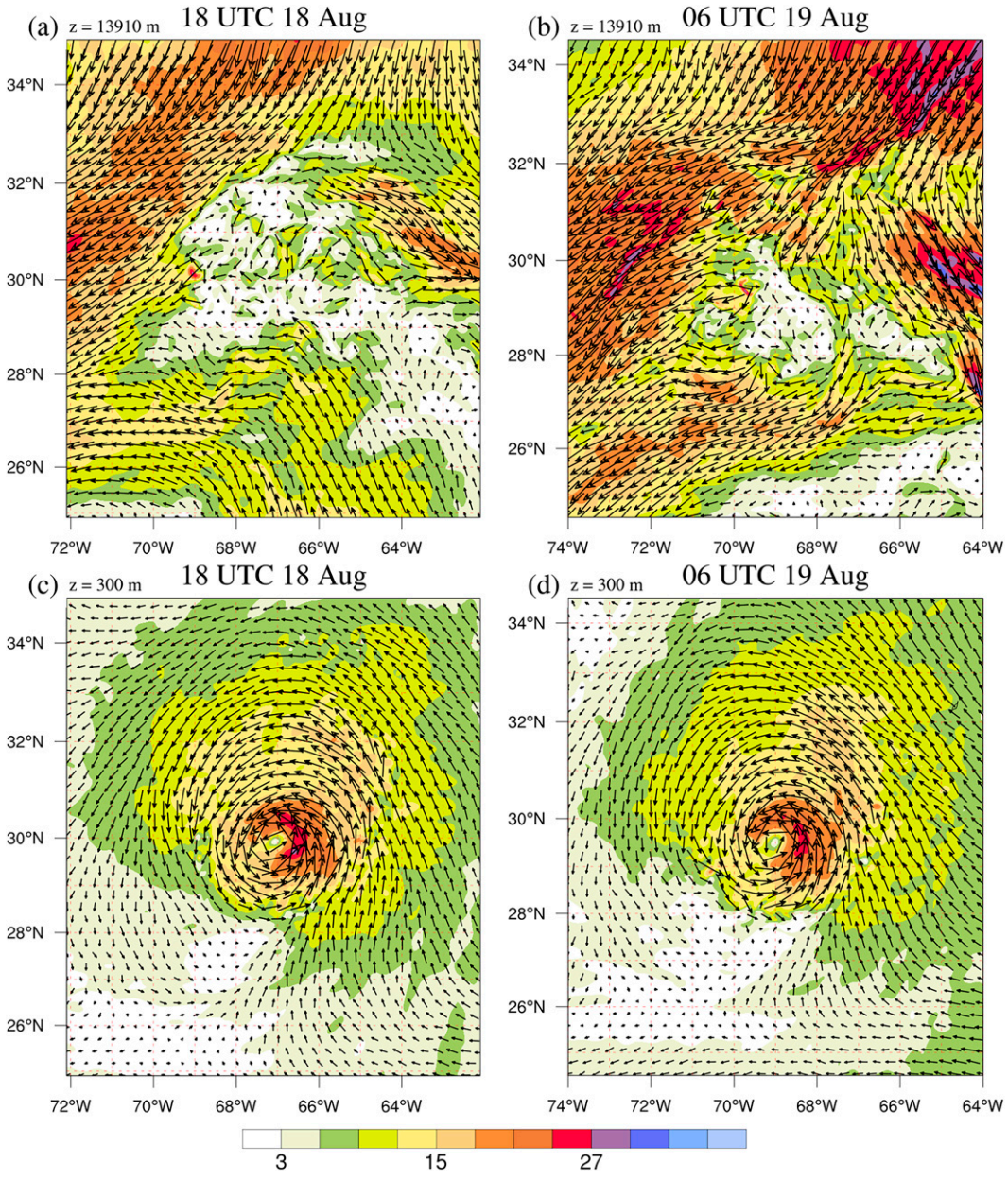

FIG. 6. Wind vectors (m s^{-1}; isotach color scale at bottom) from continuous FCDI analyses as in Figs. 4a and 4c, but for (a),(c) 1800 UTC 18 Aug and (b),(d) 0600 UTC 19 Aug.

Evans and Guishard (2009) had defined a set of criteria for identifying and classifying subtropical cyclones during the 1999–2004 Atlantic hurricane seasons. They noted that over 50% of those cyclones formed in VWS > 10 m s^{-1} in association with equatorward intrusions of upper-tropospheric troughs over relatively high sea surface temperature in the subtropics. As indicated by the upper-tropospheric flow and VWSs in Fig. 8, the VWSs in Table 2, and the $z = 300$-m vortex structures in Figs. 6c, 6d, 7c, and 7d, this is further evidence that Henri was a subtropical cyclone along its westward path.

Thus, the hypothesis is that the Henri westward path in the subtropics was due to an upper-tropospheric anticyclone that was associated with a prior Rossby wave breaking (RWB) event. Takemura and Mukougawa (2021) provided a summary of western North Pacific TC formations and subsequent tracks that have occurred in association with RWB events (Fig. 9). During the peak summer monsoon over East Asia, a large north–south potential vorticity (PV) gradient exists in association with a westerly jet stream (Fig. 9c). Rossby waves propagating eastward along the PV gradient encounter a much weaker gradient off the East Asia coast that leads to

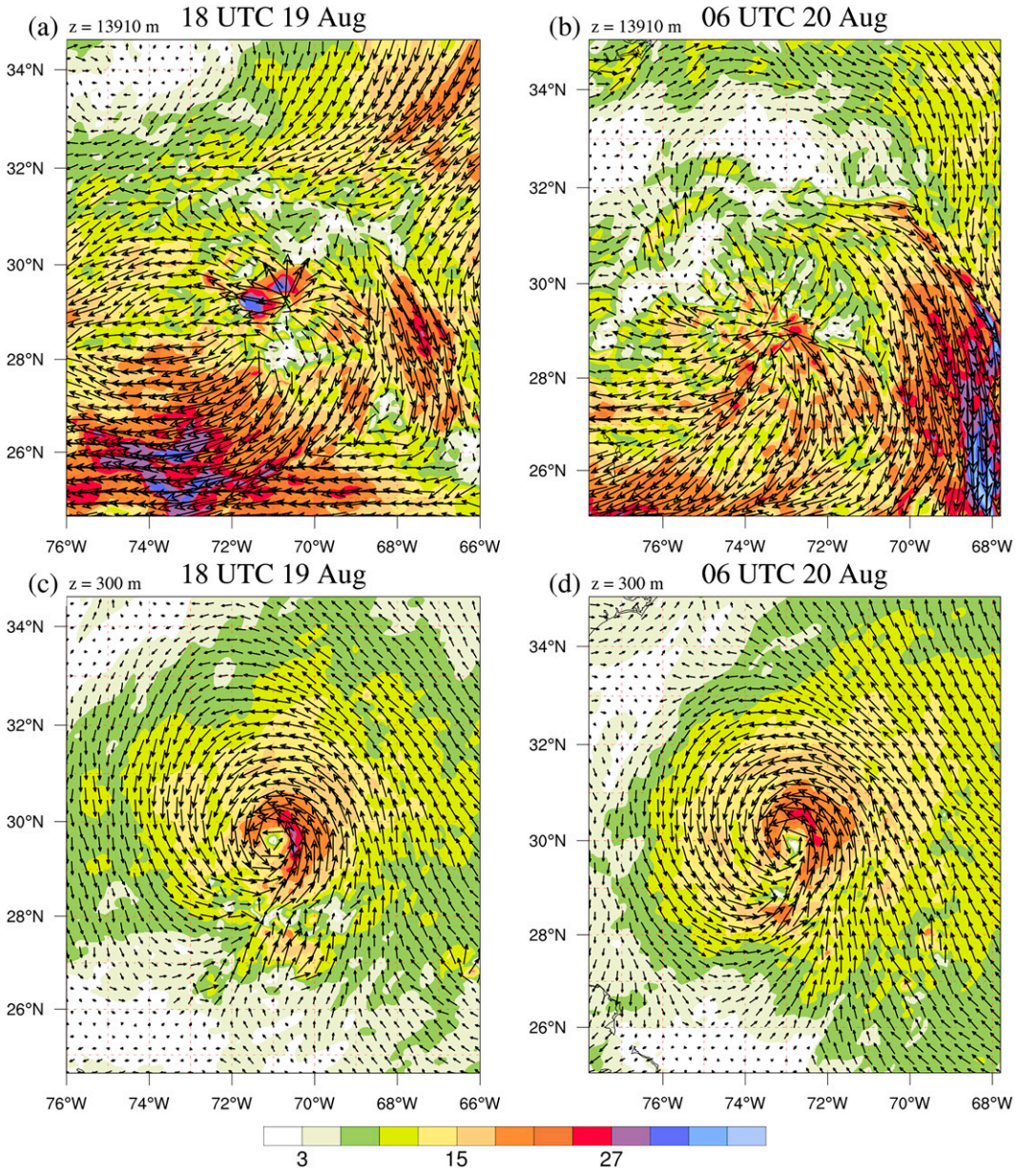

FIG. 7. Wind vectors from continuous FCDI analyses as in Fig. 6, but continuing with (a),(c) 1800 UTC 19 Aug and (b),(d) 0600 UTC 20 Aug.

RWB at the jet exit, which leads to a large PV intrusion (Fig. 9c, yellow region) southwestward toward the tropics (reference point in each panel is at 32.4°N, 160.9°E). Only a few pre-TC circulations develop at day 4 (Fig. 9d), and they tend to drift westward rather than recurve. As the RWB anticyclonic circulation amplifies and the PV intrusion extends westward at day 2 (Fig. 9e), many more TCs develop and many of those TCs have recurving tracks (Fig. 9f). When the PV intrusion has closed off at day 0 (Fig. 9g), the number of TC developments in relation to the RWB event increases and nearly all of these TCs have recurving tracks around the western boundary of that closed-off PV intrusion.

In analogy with these western North Pacific RWB events, the westward track of Henri would be along the southern boundary of the smaller, more circular anticyclonic region, labeled as "RWB ridge" in Fig. 8. Then Henri will turn poleward around the western boundary of that circular ridge in conjunction with the approach of the next shortwave trough on the western boundary of Fig. 8. It is asserted that high density upper-tropospheric AMVs will be very helpful in analyzing Atlantic RWB event impacts on TC formation, intensification, and tracks.

There is a building literature on Atlantic TC formations in relation to PV streamers (i.e., between the RWB anticyclone

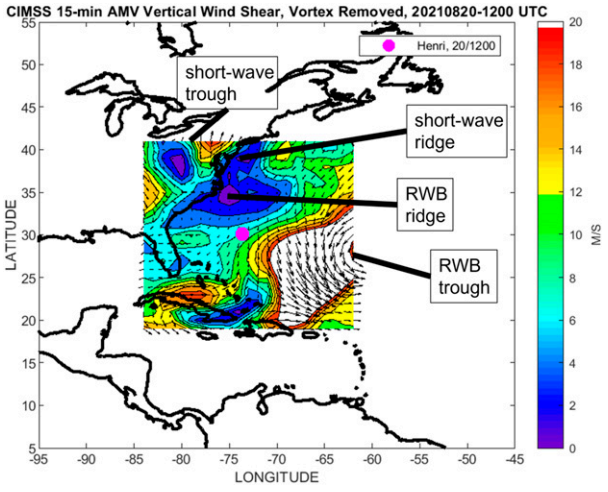

FIG. 8. Special CIMSS deep-layer vertical wind shear (VWS) vectors (m s^{-1}; color scale on right) based on high-density AMVs within the *GOES-16* mesodomain centered on the Henri vortex (magenta circle) at 1200 UTC 20 Aug. Rossby wave breaking (RWB) features are labeled.

to the north and the PV intrusion to the south), and a primarily negative influence on TC activity in the Atlantic in association with RWB events that penetrate equatorward. Galarneau et al. (2015) studied 12 TCs during 2004–08 that developed within one Rossby radius of PV streamers associated with the mid-Atlantic trough identified previously as the tropical upper-tropospheric trough. The scenario studied was the upper-tropospheric PV streamers interacting with disturbances in the lower-tropospheric easterlies, which is not relevant to the Henri westward path.

Papin et al. (2020) identify 21 149 PV streamers in the North Atlantic during June–November 1979–2015 with a peak in July–August, and define a new PV streamer index. However, their focus was on seasonal TC activity rather than relating their index to specific TC events such as the Henri case. Zhang et al. (2016) first addressed the general topic of extratropical impacts on the substantially suppressed Atlantic TC activity during August 2013. Specifically, they concluded that frequent breaking of midlatitude Rossby waves led to equatorward intrusions of cold and dry extratropical air, and consequently upper-tropospheric dryness and strong vertical wind shear. Based on the upper-tropospheric flow patterns in Figs. 6a and 6b, and the CIMSS vertical wind shears in Table 2, the environmental factors described by Zhang et al. (2016) may have played a role in the diminished intensity of subtropical cyclone Henri relative to the NHC intensities in Table 2.

Zhang et al. (2017) then separately studied RWB events in the western Atlantic versus in the eastern Atlantic. They found RWB occurrences in the western basin, which is more relevant to the Henri case, are more likely to hinder TC intensification or reduce the TC lifetime. Although these authors mention the impact of stronger vertical wind shear and reduction in the available moisture, specific examples are not provided. In a related article, Li et al. (2018) describe subseasonal variability of RWB and relate it to suppressed Atlantic TC activity on the subseasonal scale, but they do not relate it to individual events such as the Henri case.

3. Continuous FCDI analyses of the development and intensification of the mesovortex

The key to the creation of three-dimensional FCDI analyses that enable the detection of the Henri mesovortex and its environmental wind, pressure, temperature, and humidity fields is the inclusion of the high-spatial resolution *GOES-16* AMV datasets prepared by the CIMSS AMV research team at 15-min intervals. These *GOES-16* AMVs first became available at 0915 UTC 20 August, which is 3 h and 15 min after the FCDI analyses in Figs. 7b and 7d that had only hourly *GOES-16* AMVs. Although these AMV datasets are available (and utilized in the FCDI analyses) every 15 min within the *GOES-16* mesodomain as in Fig. 8, publication space limitations restrict the presentation to synoptic times and synoptic times + 3 h.

At 1200 UTC 20 August (Fig. 10, top left), the enhanced *GOES-16* upper-tropospheric AMVs reveal two outflow bursts (red AMVs emanating radially from a vortex area to become anticyclonically turning green vectors at larger radii). The largest, and most symmetric outflow burst centered near 29.5°N, 73.3°W is well to the southeast of the main Henri vortex at 30.2°N, 73.7°W. Indeed, one of the strongest, most coherent branches of this outflow is directly over the main vortex position, and this is when the Air Force Reserve U2 mission had reported at 1141 UTC 20 August (Table 1) a maximum surface wind of only 37 kt, (NHC WBT had 55 kt, Fig. 1). The second, smaller outflow burst was nearly coincident with the FCDI-analyzed z = 300-m mesovortex center near 29°N, 74°W, which is more than 130 km to the south of the main Henri vortex. The main branch of this second outflow burst is toward the southwest and emanates very near the center, which is interpreted to mean it is a newer outflow burst than the larger outflow burst to the southeast of the main Henri vortex. The southwestward orientation of the southern (mesovortex) outflow burst may be attributed to the VWS-C, which is from the northeast according to the *GOES-16* AMV version in Fig. 8.

At 1500 UTC 20 August (Fig. 10, top right) the leading edge of the first outflow burst from 3 h earlier has spread northward to 31.5°N and the outflow in the eastern semicircle is quite coherent. Within the central region of the first outflow burst, the large white spaces indicate this first outflow burst is near its ending phase. Note that the main Henri vortex still has relatively strong radial outflow directly overhead. The southern (mesovortex) outflow burst is spreading mainly to the south and to the southeast so that the leading edge is along 28°N. Although it is unknown as to the time these two outbursts began because the 15-min *GOES-16* AMVs began only 3 h earlier, it appears the life cycle may only be 6–12 h.

At 1800 UTC 20 August (Fig. 10, bottom left), the original first outflow burst has spread out and weakened, and a new outflow burst originating near 30.2°N, 73.2°W is spreading

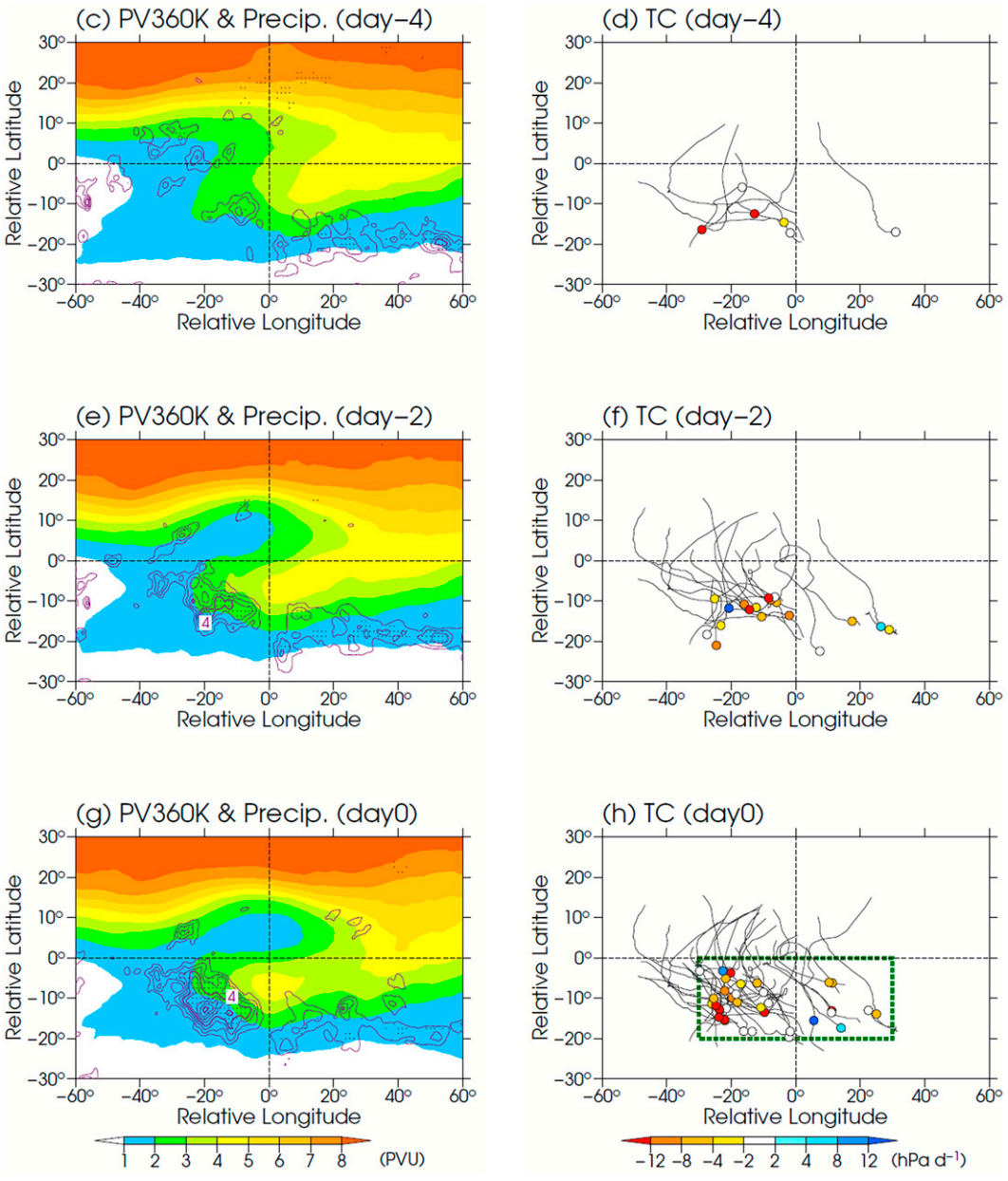

FIG. 9. Modified composites by Takemura and Mukougawa (2021) of (left) 300-K potential vorticity (PV) and (right) relative positions of TC developments (circles) and subsequent tracks (gray lines) relative to the coordinate origin that corresponds to the Rossby wave breaking (RWB) center at 32.4°N, 160.9°E. (c),(d) Day 4, (e),(f) day 2, and (g),(h) day 0 relative to the peak frequency of TC developments. See (a) and(b) in Takemura and Mukougawa (2021) for additional details.

northwestward and eastward. The leading edge of the mesovortex outflow burst is still evident to the south along 28°N, and a narrow outflow burst to the east can be traced back to the location of the mesovortex. Just 3 h later at 2100 UTC 20 August (Fig. 10, bottom right) the new outflow burst that is centered a little farther to the west near 30.2°N, 73.5°W has rapidly spread toward the east-northeast, but it also has less-strong outflow branches toward the north and toward the east. Note that the main Henri vortex is still within the western edge of the northward-oriented AMVs associated with the outflow burst to the south, which inhibits intensification. However, outflow toward the north above the main Henri vortex has increased, which is favorable for intensification. The new outflow burst above the southern mesovortex has again spread to the south and to the southeast, and those AMVs toward the southeast have a more direct link to the jet streak in the southeastern corner of the mesodomain, which is favorable for intensification (Fig. 10, bottom right).

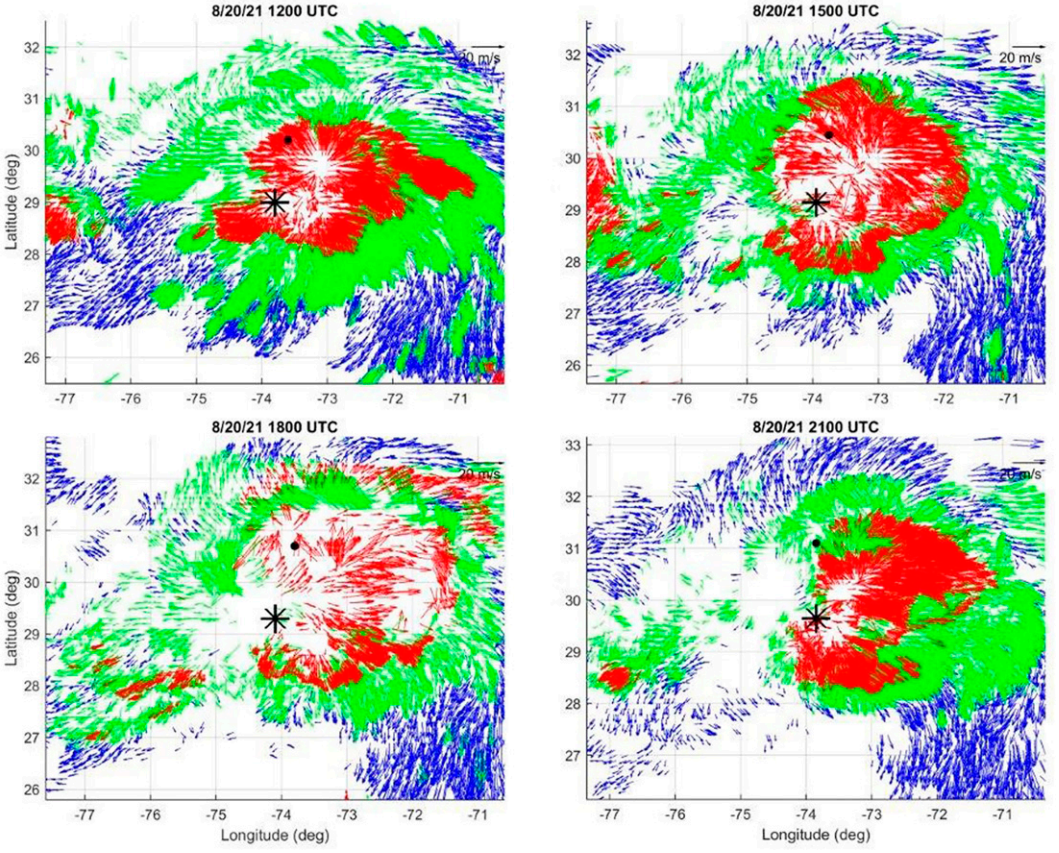

FIG. 10. The 3-hourly sequence (dates and times included at top) of 15-min, high spatial resolution *GOES-16* AMVs prepared by CIMSS during Henri, with red vectors within the 100–150-mb layer, green vectors within the 150–200-mb layer, and blue vectors within the 200–250-mb layer. The position of the main Henri vortex is indicated by the black dot, and position of the southern mesovortex is indicated by the black asterisk.

a. Discovery of multiple low-level mesovortices

While 15-min *GOES-16* AMV datasets such as at 1200 UTC 20 August are continuously inserted in the FCDI analyses, the impacts of the outflow bursts as in Fig. 10 (top left) likely require hours to spread throughout the entire troposphere. As described in section 1a, it is the difference between the AMV u and v wind components and the COAMPS model u and v wind components that becomes the nudging term in the dynamic initialization step. The AMV datasets are held constant for each 15-min FCDI time interval, but the next AMV dataset must be quite similar for the nudging to continue to force the model wind components to approach the magnitudes and directions of the AMV dataset. Thus, it may require many more 15-min periods before the lower-tropospheric mass-pressure fields adjust to such large wind field perturbations associated with an outflow burst aloft.

Note that the implication here is that these are environmental "top-down developments" of low-level mesovortices that may later undergo RI—rather than "bottom-up developments" in which the intense low-level mesovortices that have associated deep convection that later lead to an outflow burst aloft. As was illustrated by Elsberry et al. (2020, their Fig. 1), only the 15-min *GOES-16* AMVs in the mesodomain have the temporal and spatial resolution to resolve the magnitude and time evolution of the outflow bursts as in Fig. 10. The hourly *GOES-16* AMVs incorporated into many global and regional numerical models resolve only the outer region of the outflow burst and have less spatial resolution.

The accumulated effect of the ongoing outflow bursts from 1200 UTC 20 August to 2100 UTC 20 August as revealed in the corresponding FCDI analysis wind vectors from 1200 UTC 20 August are displayed in Figs. 11, 12a, and 12b at z = 13 910 m and Figs. 12c and 12d at z = 300 m. Note in Fig. 11a that there are three outflow bursts at z = 13 910 m with isotach magnitudes exceeding 21 m s^{-1} within the region 29°–30°N, 73°–74°W. The strongest (>30 m s^{-1}) is the outflow burst toward the east and southeast that is associated with the mature AMV outburst in Fig. 10 (top left), which is also to the south of the z = 300-m main Henri vortex near 30.2°N, 73.8°W (Fig. 11c). However, there is a separate low-level mesovortex developing in a region of converging wind vectors where the western inner isotach maximum of the subtropical Henri is now approaching the longer eastern isotach band that is extending well to the south. The early stage of the southern mesovortex that is displayed in Fig. 4 (left column) is developing

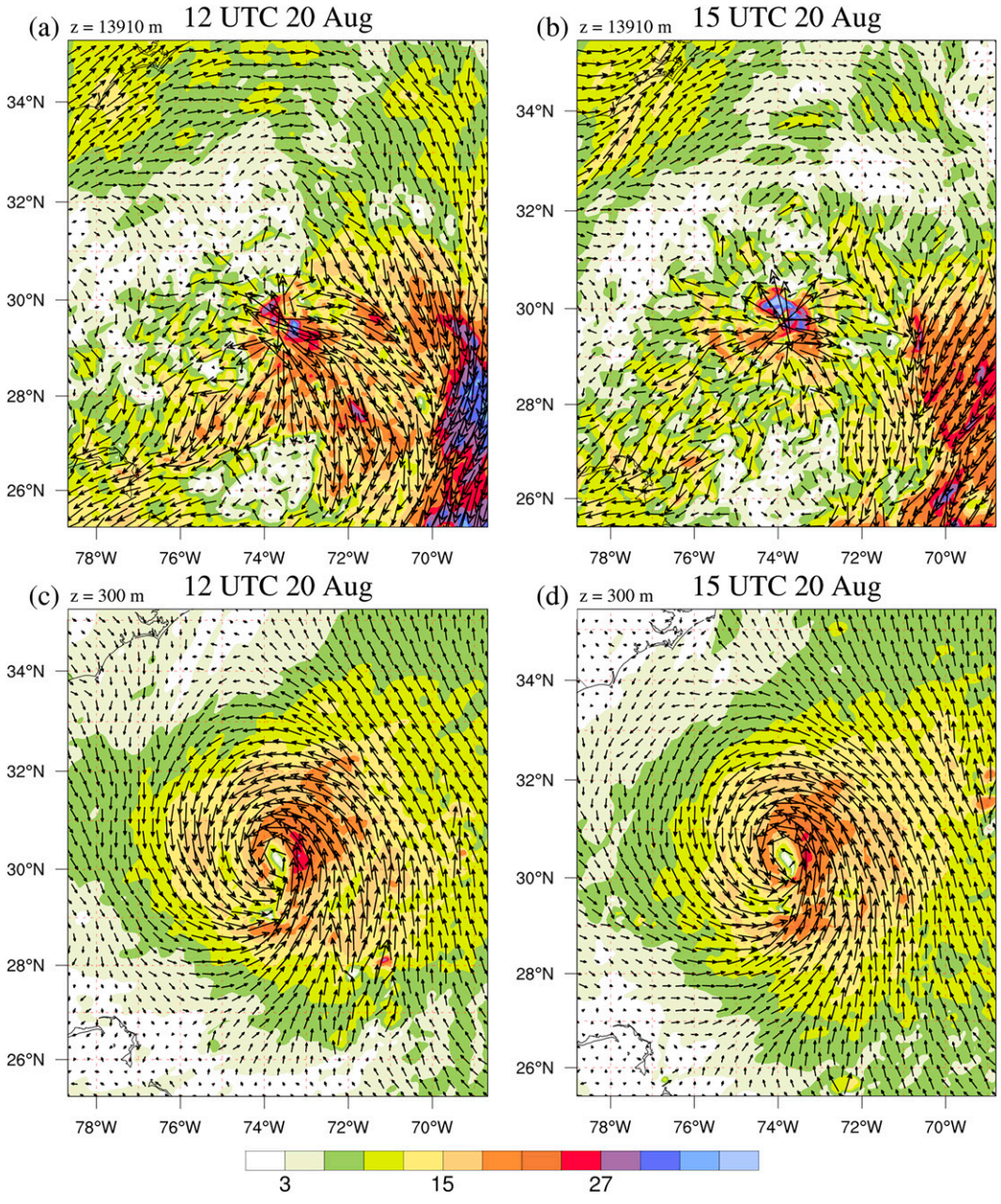

FIG. 11. Wind vectors (m s^{-1}) from continuous FCDI analyses as in Figs. 4a and 4c, but for (a),(c) 1200 UTC 20 Aug and (b),(d) 1500 UTC 20 Aug corresponding to the *GOES-16* AMVs in the top left and top right panels of Fig. 10, respectively.

in a region of converging vectors farther to the south near 29°N, 74°W where the western outer isotach maximum of the subtropical Henri is interacting with that southward extension of the long eastern isotach band. It is unclear what relationship the third outflow burst near 30°N, 74.2°W has with the AMVs in Fig. 10 (top left), or with the main Henri vortex in Fig. 11c. A separate weaker radial outflow near 29.2°N, 73.8°W (Fig. 11b) appears to be directly above the z = 300-m mesovortex well to the south of the main Henri vortex (Fig. 11d). During the past 3 h (i.e., compared to Fig. 11c) the wind speeds to the southeast of this mesovortex have increased and these stronger winds have spread over a larger area.

The 3-hourly sequence of FCDI analyses is continued in Fig. 12 with the 1800 UTC 20 August analyses in the left column and the 2100 UTC 20 August analyses in the right column. The 1800 UTC 20 August FCDI analysis at z = 13 910 m in Fig. 12a has an outer ring of strong (>15 m s^{-1}) near-radial

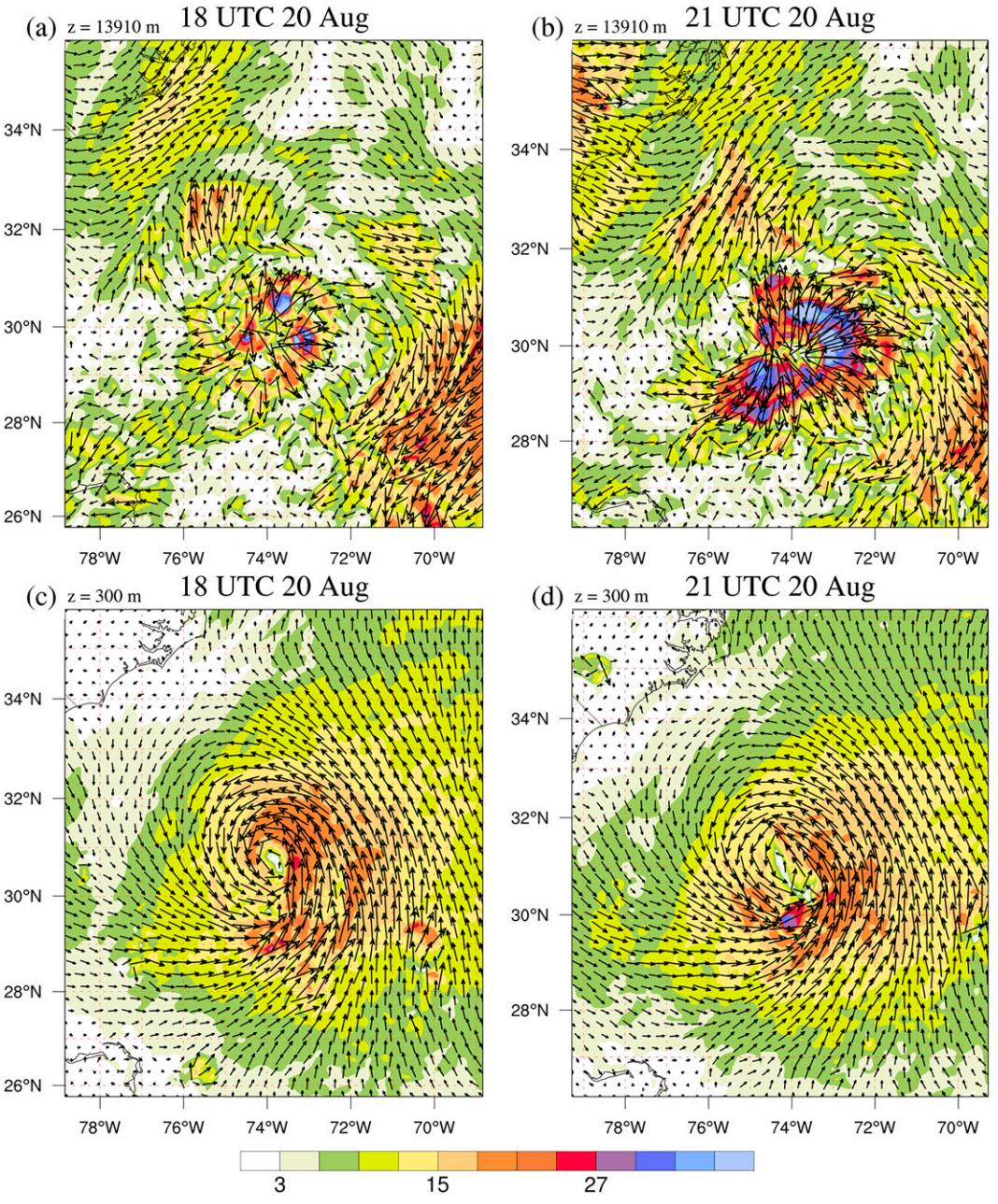

FIG. 12. Wind vectors (m s^{-1}) from continuous FCDI analyses as in Figs. 4a and 4c, but for (a),(c) 1800 UTC 20 Aug and (b),(d) 2100 UTC 20 Aug corresponding to the *GOES-16* AMVs in the bottom left and bottom right panels of Fig. 10, respectively.

wind vectors that represent the outer ring of green (150–200 mb) *GOES-16* AMVs in Fig. 10 (bottom left). Embedded within that FCDI outer ring are three isotach maxima (>30 m s^{-1}) that are consistent with three clusters of red (100–150 mb) *GOES-16* AMVs in Fig. 10 (bottom left). As in the previous FCDI analysis (Fig. 11b), the outflow bursts to the north and to the east are the strongest, but the outflow burst to the south of the main Henri vortex has grown stronger. There is still an inner mesovortex signature at the south end of the main Henri vortex (Fig. 12c) that may be associated with the northern outflow burst isotach maximum in Fig. 10 (bottom left). However, the best signature of a mesovortex is near 29.4°N, 74.0°W well to the south of the main Henri vortex.

Recall from the *GOES-16* AMVs at 2100 UTC 20 August (Fig. 10, bottom right) the new very strong outflow burst to the east and the new smaller, but strong outflow burst in association with the southern mesovortex. The intensification and the near-radial outward wind vectors to the east and to the south of these

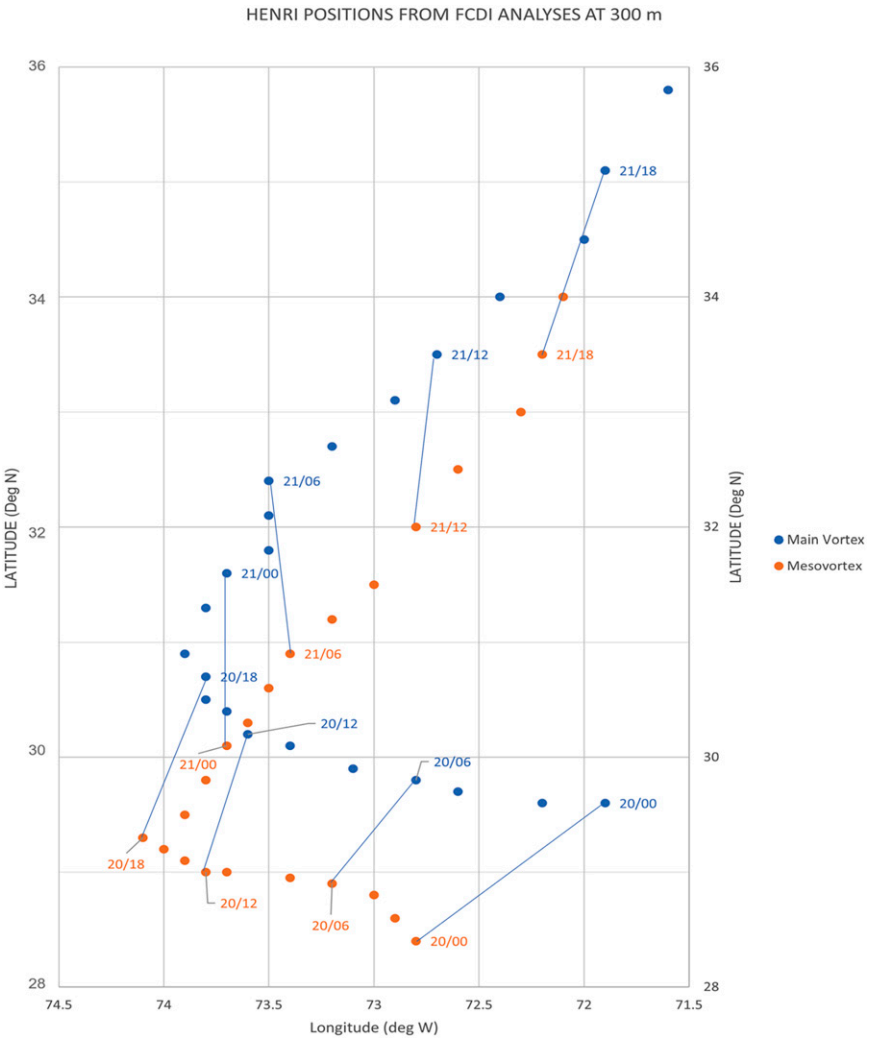

FIG. 13. Detected center positions in the z = 300-m FCDI analyses at the 2-h intervals (labeled and connected with blue lines at 6-h synoptic times of DD/HH on 20–21 Aug 2021) for the main Henri vortex (blue dots) and for a southern mesovortex (red dots) that is the focus of this study.

outflow bursts are well represented in the z = 13 910-m FCDI analysis at 2100 UTC 20 August (Fig. 12b). Similarly, there are two separate mesovortices in the z = 300-m FCDI analysis (Fig. 12d). The inner mesovortex centered near 30.2°N, 73.6°W has greatly expanded during the last 3 h, while the main Henri vortex has decreased in intensity. Meanwhile, the southern mesovortex has rapidly intensified to 30 m s^{-1} and the isotach maximum has continued to expand in areal extent.

The spatial relationships between the positions of the main Henri vortex and the positions of the southern mesovortex, which is the primary focus of this study, are displayed in Fig. 13 (blue dots and red dots, respectively). Recall that the main vortex center positions generally match well the NHC best track positions due to the surface wind adjustment procedure of Elsberry et al. (2020) now applied to the Henri case. Note that some evidence of a southern mesovortex existed in the z = 300-m FCDI analyses as early as 0000 UTC 20 August, but all of these FCDI analyses prior to 1200 UTC 20 August only had hourly *GOES-16* AMVs available. Consequently, the vortices are broader and the positions prior to 1200 UTC 20 August have greater uncertainty, and thus will not be discussed.

During the 1200–2100 UTC 20 August period of Figs. 10–12, the translation speed of the main Henri vortex slowed and the direction turned to the north. Similarly, the southern mesovortex slowed, reached its maximum westward position at 1800 UTC 20 August, and then sharply changed direction to a more northward path to again be parallel to the path of the main Henri vortex. Note that the mesovortex path has been analyzed to cross over the path of the main Henri vortex after 0000 UTC 21 August.

b. *Continuous FCDI analyses during and following Henri's poleward turn*

The poleward turn of the main Henri vortex after 2000 UTC 20 August (Fig. 13) was in response to the approach of a shortwave trough with a leading edge revealed at 0000 UTC

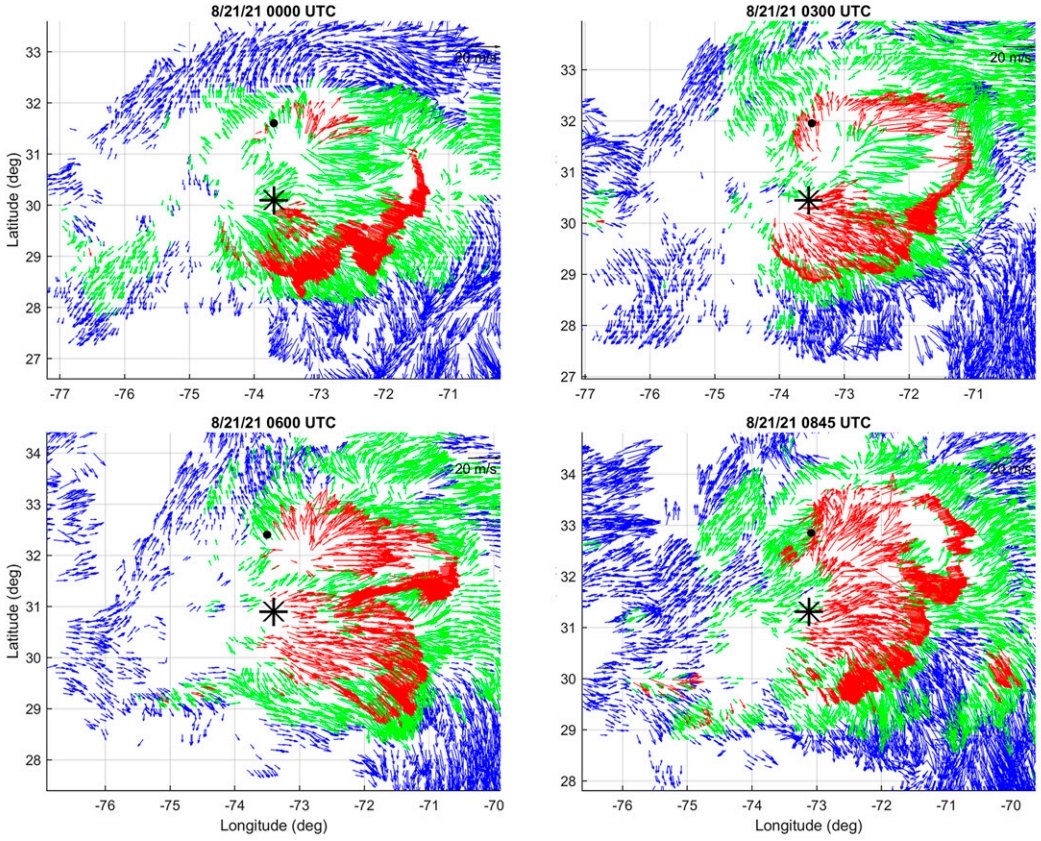

FIG. 14. The 3-hourly sequence (dates and times included at top) of 15-min, high spatial resolution *GOES-16* AMVs as in Fig. 10.

21 August by the 200–250-mb layer AMVs (blue) in the northwest corner of Fig. 14 (top left). An outflow burst is indicated near 31°N, 73.5°W, which is to the southeast of the z = 300-m main Henri vortex (black dot). The second outflow burst is centered just to the west of the southern mesovortex (black asterisk), and has fan-shaped radial outflows ranging from southeastward to eastward, and even some small northeastward vectors. Note in Fig. 14 (top left) that for the first time the southeastward directed outflow extends to at least 27°N to merge with the trough that is designated as the "RWB trough" in Fig. 8. Such direct connections of outflows with adjacent synoptic flows were shown by Elsberry et al. (2020) to be correlated with sustained intensification periods of Hurricane Irma (2017), and the southern mesovortex was intensifying during this period with the outflow directly connected to that RWB trough.

The corresponding 0000 UTC 21 August FCDI analyses at z = 13 910 m and z = 300 m are displayed in Figs. 15a and 15c, respectively. There are actually two nearby centers along 74°W from which radially outward wind vectors are emanating, and there are two near-circular isotach maximum rings with diameters of about 1° latitude and 2° latitude (Fig. 15a). Note also the connection of these Henri-associated outflows with the jet streak along the leading edge of the shortwave trough in the northwest corner of Fig. 15a. While the inner mesovortex was dominant over the main Henri vortex 3 h previously (Fig. 12d), these two circulations appear to have merged at 0000 UTC 21 August. It is noteworthy that the southern center within the expanding outflow burst in Fig. 15a is directly over the z = 300-m southern mesovortex that is the focus of this study (Fig. 15c). The implication is that that southern mesovortex will be intensifying during the next few hours.

Just 3 h later (0300 UTC 21 August), the shortwave trough has advanced toward the main Henri vortex, which has enhanced the jet streak direct connection with the northward outflow from that vortex (Fig. 14, top right). However, with the center of an outflow burst still to the southeast of that vortex center, a branch of the 100–150-mb (red) outflow is directly over that main Henri vortex and decreased intensity should be anticipated. By contrast, a new 100–150-mb outflow burst is emanating from above the southern mesovortex, and its southward outflow branch has extended below 28°N. The z = 13 910-m continuous FCDI analysis (Fig. 15b) has both the enhanced direct connection with the shortwave jet streak and an overall strengthening of the outflow burst above that mesovortex (especially toward the east and to the south). The associated changes in the z = 300-m FCDI analysis (Fig. 15d) include: (i) the intensity of the main Henri vortex decreased; (ii) an extended north–south region of light winds the size of the main vortex eye region developed along the cyclonic side

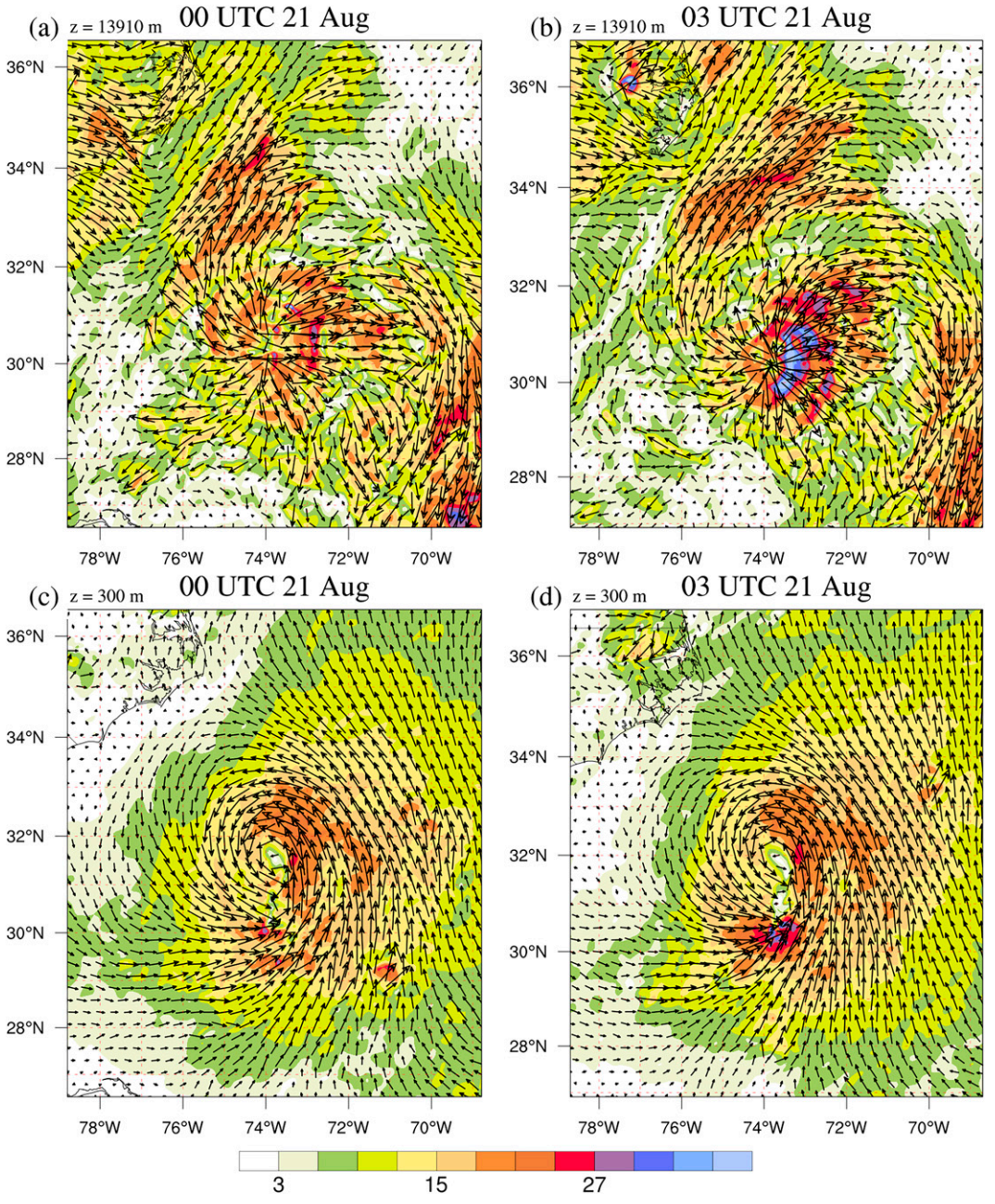

FIG. 15. Wind vectors (m s^{-1}) from continuous FCDI analyses as in Figs. 4a and 4c, but for (a),(c) 0000 UTC 21 Aug and (b),(d) 0300 UTC 21 Aug corresponding to the *GOES-16* AMVs in the top-left and top-right panels of Fig. 14, respectively.

of the isotach band between the main vortex and the southern mesovortex; and (iii) the southern mesovortex intensified rapidly during the past 3 h (i.e., compare with Fig. 15c wind vectors), and the region of maximum winds to the south of that mesovortex center greatly expanded.

At 0600 UTC 21 August, which is the time of the FCDI analyses of the southern mesovortex in Fig. 4 (left column), a new northern outflow burst still centered to the southeast of the main Henri vortex is revealed in the high spatial and temporal resolution *GOES-16* AMVs (Fig. 14, bottom left). Note that the strongest outflow is toward the northeast. The shortwave trough has advanced eastward such that an outflow branch toward the north-northwest above the main Henri vortex feeds directly into the shortwave jet streak. The outflow burst associated with the southern mesovortex that was initiated around 2100 UTC 20 August (Fig. 10, bottom right), and was continued at 0000 and 0300 UTC 21 August (Fig. 14, top left and top right), has further extended to the southeast

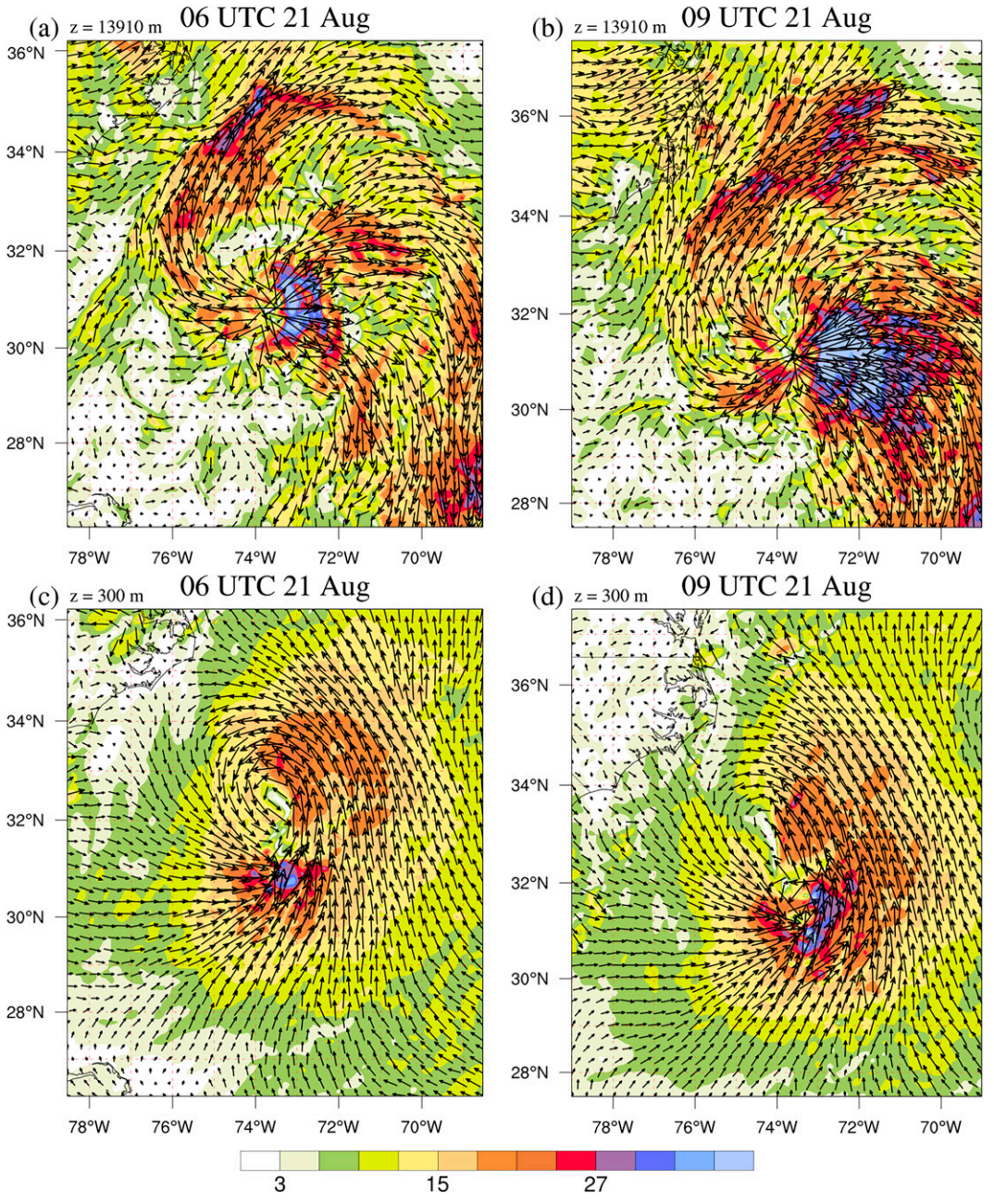

FIG. 16. Wind vectors (m s^{-1}) from continuous FCDI analyses as in Figs. 4a and 4c, but for (a),(c) 0600 UTC 21 Aug and (b),(d) 0900 UTC 21 Aug corresponding to the *GOES-16* AMVs in the bottom-left and bottom-right panels of Fig. 14, respectively.

(bottom-left panel). Note that very high (red, 100–150 mb) AMVs extend to about 2° latitude to the south and 2° longitude to the east of the southern mesovortex, which is leading to a strong direct connection with the RWB trough as in Fig. 8.

The continuous FCDI analyses at 0600 UTC 21 August in Fig. 4 are repeated in Figs. 16a and 16c to show the continuity with the 0300 UTC 21 August FCDI analyses (Figs. 15b,d). The westward wind vectors out of the outflow burst turn anticyclonically to join the >30 m s^{-1} jet streak near 35°N, 74°W. As indicated in section 1d, the poleward vectors from the outflow burst at 0600 UTC 21 August extended only a short distance before terminating in a subsidence region along 32°N. That is, this is where the northward outflow had interacted with the southward outflow associated with the main Henri vortex, which has an elongated southeast–northwest center (Fig. 16c) near 32.2°N, 73.5°W, although the main vortex center positions between 0000 and 0600 UTC 21 August were difficult to estimate (Fig. 13).

The most noteworthy feature in the z = 13 910-m FCDI analysis in Fig. 15b is the two outflow burst branches with >30 m s^{-1} wind vectors to the northeast and to the southeast as were observed in the *GOES-16* AMVs in Fig. 14 (bottom left). The outflow burst branch to the northeast curves anticyclonically to join a weak northerly jet east to 70°W. The primary outflow burst branch to the southeast makes a more direct connection to a northerly jet near 28°N, 72°W, which is generally consistent with the long extension to the southeast of the 100–150-mb AMVs in Fig. 14 (bottom left).

When we first examined the 6-hourly outputs of the continuous FCDI analyses and discovered the strong southern mesovortex at 0600 UTC 21 August as in Fig. 4 (left column), we noted that at 1002 UTC 21 August the southern mesovortex seemed to have weakened as it blended into the long isotach maximum extending to the south from the region of the main Henri vortex. However, the *GOES-16* AMVs at 0845 UTC 21 August (Fig. 14, bottom right) clearly indicate that the 100–150-mb AMVs have continued to pour out of the top of the southern mesovortex, and all along a line up to the main vortex, and spread hundreds of kilometers throughout the eastern semicircle. Note that the southern mesovortex-related AMVs continue to have a direct connection with the upper-tropospheric RWB trough to the southeast by more than 3° latitude and longitude. This strong direct connection between the southern mesovortex outflow and that RWB trough can be traced backward through the earlier 3-hourly panels in Figs. 16a and 16b to the 2100 UTC 20 August AMVs in Fig. 10 (bottom right).

The continuous FCDI analysis of z = 13 910-m wind vectors at 0900 UTC 21 August in Fig. 16d depict well the outflow burst from the southern mesovortex throughout the eastern semicircle, and also a direct connection of the westward outflow with an extensive jet streak to the northwest and north. In response, the z = 300-m FCDI wind vectors (Fig. 16d) indicate an intensification of the mesovortex and along a north–south line generally coincident with the largest eastward outflow at z = 13 910 m. Note that the main Henri vortex is analyzed as a northwest–southeast region of light winds with the center near 33°N, 74°W adjacent to maximum winds > 21 m s^{-1}.

4. Summary and discussion

a. Summary

Henri (2021) was one of the aircraft mission objectives of the ONR Tropical Cyclone Rapid Intensification (TCRI) field experiment in collaboration with the NOAA APHEX, and the CIMSS provided high spatial and temporal (15-min) resolution *GOES-16* AMVs from 0915 UTC 20 August. The two Henri phases of interest in this study are first when TS Henri moved westward along 30°N, and second when around 0000 UTC 20 August Henri turned poleward and moved to the north-northwest. Almost all of the regional numerical weather prediction models, and the NHC, predicted that Henri would become a hurricane by 0000 UTC 21 August (Fig. 1). The NHC intensity best track (Pasch et al. 2021) does have Henri as a hurricane at 1200 UTC 21 August. However, six Air Force Reserve aircraft fixes for Henri between 1800 UTC 19 August and 1600 UTC 22 August did not have maximum surface winds over 55 kt, and most of these intensity fixes were closer to a weak TS. These Air Force Reserve intensity fixes provide evidence that the main Henri vortex did not rapidly intensify, and likely decreased in intensity during the turn poleward. Another departure from the NHC best track description of Henri was the discovery in our continuous FCDI analyses of a rapidly intensifying mesovortex to the south of the main Henri vortex, which occurred at the same time as that main vortex was decreasing in intensity in the FCDI analysis. Thus, the primary objective of this study was to create a high temporal (15-min) validation dataset from the FCDI analyses with the *GOES-16* AMVs to analyze both the period of the unusual westward track along 30°N and the development and rapid intensification of the mesovortex.

Whether initiated without the hourly *GOES-16* AMVs in a sequence of 6-hourly Control COAMPS-TC forecasts, or in the FCDI analyses with those AMVs, the diagnosed maximum intensities during the westward path of Henri are consistently 5–10 m s^{-1} smaller than the NHC best track intensities. These smaller maximum intensities are more consistent with the Air Force Reserve aircraft fixes, and are also more consistent with the satellite-based CIMSS vertical wind shears of 20–30 kt during most of that westward Henri path. Furthermore, the FCDI z = 300-m wind analyses demonstrate highly asymmetric wind fields and a horseshoe-shaped isotach maximum (~21 m s^{-1}) that is about 75 km from the center. These two characteristics of the Henri vortex are more consistent with the NHC definition of a subtropical cyclone in section 2, as might be expected for a cyclone whose origin was north of 30°N, rather than a TC. It was not until 0600 UTC 20 August (i.e., just prior to the northward turn of Henri) that the wind field in the FCDI analyses is more symmetric (comma-shaped isotach maximum) that more resembles a TC than a subtropical cyclone.

Another advantage of the 15-min *GOES-16* AMV datasets is that the CIMSS AMV team can provide high spatial and temporal resolution vertical wind shear fields for the Henri case after 0900 UTC 20 August. This was the beginning of Henri's poleward turn after a westward path between a ridge to the north and a strong trough to the south, which is analogous to the Rossby wave breaking (RWB) conceptual model of Takemura and Mukougawa (2021). The passage of a shortwave ridge and shortwave trough to the north of the RWB ridge that would contribute to the Henri RWB event is revealed in the FCDI analyses during the Henri westward path.

Fortunately, the 15-min *GOES-16* mesodomain AMVs were available during and following the Henri turn to the north when the mesovortex formed to the south. The high spatial resolution of those AMVs in the 100–150-, 150–200-, and 200–250-mb layers allow the visualization of the outflow bursts in space and time (here, 3-hourly, but could be 15 min) in association with the southern mesovortex development and intensification. Then the FCDI analyses forced by those thousands of AMVs each 15 min depict the z = 13 910-m wind

field responses and the subsequent z = 300-m wind field adjustments in the southern mesovortex.

The unexpected result from the continuous FCDI analyses was that there were multiple inner-region mesovortices associated with individual outflow bursts aloft between 1200 and 1800 UTC 20 August, when there were three outflow bursts within an outer burst ring (Fig. 12a). The southern mesovortex had also expanded and intensified just as it approached the prior westward path of the main vortex (Fig. 13). It is noteworthy during that time there were continually radial outflow vectors passing over the region of the main Henri vortex, which is consistent with a decay in time.

The period when the southern mesovortex was crossing what is expected to have been an ocean-cooled region to the right of the path of the main Henri vortex was when the outflow burst above that mesovortex became continuous in time and quite strong (Fig. 14). Thus, the southern mesovortex at z = 300 m became more and more intense (Figs. 15 and 16). The northern outflow burst also was persistent in time (Fig. 14), and continued to be displaced to the southeast of the main Henri vortex. A persistent and strong mesovortex was also below the northern outflow burst. It was when the two outflow bursts joined (Fig. 16b) to create eastward radial outflow all along the line between them that the southern mesovortex reached maximum intensity and maximum size (Fig. 16d).

b. Discussion

The continuous FCDI analyses from 0000 UTC 18 August first with hourly *GOES-16* AMVs provides a different perspective on the Henri structure and intensity during its westward path than in the NHC best track. Specifically, the FCDI analyses depict Henri as a subtropical cyclone with a highly asymmetric low-level wind field of lower maximum wind speeds at 75 km analogous to the NHC definition. Since in situ aircraft observations were not available until 1800 UTC 19 August during that westward path, the NHC satellite-based intensity estimates (Fig. 3) are almost exclusively from highly variable Dvorak and automated Dvorak technique (ADT) estimates with only a few scatterometer estimates. By contrast, the hourly AMVs are continually monitoring the Henri outflow with the adjacent synoptic circulations, and the continuous FCDI analyses adjust the three-dimensional wind fields of Henri to that forcing. The FCDI analyses also have the constraint of the surface wind adjustment that moves a 0–1500-m layer of the wind field along the target 6-h path from the NHC WBT, which ensures that the origins of central deep convection are also constrained.

With these high temporal resolution (15 min, but here displayed either at 2- or 3-h intervals) FCDI analyses, it is clear that the development and spreading out of the outflow bursts aloft precedes the intensification of the mesovortices below. For these subtropical Henri mesovortices, the outflow burst associated with the mesovortex developments and intensifications were not accompanied by subsidence in a small ring above the mesovortex center. Rather, these mesovortices had associated outflow bursts (warm air) that had direct connections with adjacent synoptic circulations (cold troughs) such that the warm air continues to accelerate down the side of the outflow burst. In the case of subtropical Henri (Fig. 8), the Rossby wave breaking trough was the adjacent cold air.

The continuous FCDI analyses with high temporal resolution *GOES-16* AMVs in the mesodomain for "unusual" (Pasch et al. 2021) subtropical Henri are just one example of the opportunity for improved understanding of RI events that was the objective of the ONR TCRI field experiment during 2021. Examinations of RI events in other TCs observed during the 2021 field experiment are in progress. Although not displayed here, COAMPS-TC forecasts initiated from these FCDI analyses as initial conditions start smoothly and provide better forecasts of rapidly developing outflow bursts than Control forecasts with the standard initialization each 6 h. Thus, the continuous FCDI analyses including the high temporal resolution *GOES-16* AMVs within the mesodomain would be expected to provide improved TC track and intensity forecasts.

Acknowledgments. This is a collaborative ONR Project N000142012180 (RLE) and N0001421WX00579 (JWF, HJC) in coordination with CIMSS (CSV). Our thanks to the ONR TCRI leadership in conjunction with the NOAA HRD leadership for arranging the missions into Subtropical Cyclone Henri, and a special thank you to the Air Force Reserve crews that obtained the aircraft observations of Henri that were critical for this study. The CIMSS AMV team are thanked for providing the special *GOES-16* AMV datasets and responding to our questions. Dr. Sue Chen of Naval Research Laboratory—Monterey provided Fig. 1 and inputs related to the potential vorticity fields during RWB events. We also thank Navy DSRC located at the NASA Stennis Space Center who provided computational resources through the HPCMP to our project. The authors are not aware of any conflicts of interest.

Data availability statement. The Henri *GOES-16* AMVs are available from CIMSS upon request. The Air Force Reserve aircraft observations are available at https://nhc.noaa.gov/archive/recon/2021/.

REFERENCES

Elsberry, R. L., E. A. Hendricks, C. S. Velden, M. M. Bell, M. Peng, E. Casas, and Q. Zhao, 2018: Demonstration with special TCI-15 datasets of potential impacts of new-generation satellite atmospheric motion vectors on Navy regional and global models. *Wea. Forecasting*, **33**, 1617–1637, https://doi.org/10.1175/WAF-D-17-0168.1.

——, J. W. Feldmeier, H.-J. Chen, M. Peng, C. S. Velden, and Q. Wang, 2020: Challenges and opportunities with new generation geostationary meteorological satellite datasets for analyses and initial conditions for forecasting Hurricane Irma (2017) rapid intensification event. *Atmosphere*, **11**, 1200, https://doi.org/10.3390/atmos11111200.

Evans, J. L., and M. P. Guishard, 2009: Atlantic subtropical storms. Part I: Diagnostic criteria and composite analysis.

Mon. Wea. Rev., **137**, 2065–2080, https://doi.org/10.1175/2009MWR2468.1.

Galarneau, T. J., R. McTaggart-Cowan, L. F. Bosart, and C. A. Davis, 2015: Development of North Atlantic tropical disturbances near upper-level potential vorticity streamers. *J. Atmos. Sci.*, **72**, 572–597, https://doi.org/10.1175/JAS-D-14-0106.1.

Lewis, W. E., C. S. Velden, and D. Stettner, 2020: Strategies for assimilating high-density atmospheric motion vectors into a regional tropical cyclone forecast model (HWRF). *Atmosphere*, **11**, 673, https://doi.org/10.3390/atmos11060673.

Li, W., Z. Wang, G. Zhang, M. S. Peng, S. G. Benjamin, and M. Zhao, 2018: Subseasonal variability of Rossby wave breaking and impacts on tropical cyclones during the North Atlantic warm season. *J. Climate*, **31**, 9679–9695, https://doi.org/10.1175/JCLI-D-17-0880.1.

Papin, P. P., L. F. Bosart, and R. D. Torn, 2020: A feature-based approach to classifying summertime potential vorticity streamers linked to Rossby wave breaking in the North Atlantic basin. *J. Climate*, **33**, 5953–5969, https://doi.org/10.1175/JCLI-D-19-0812.1.

Pasch, R. J., R. Berg, and A. B. Hagen, 2021: Tropical cyclone report: Hurricane Henri (15–23 August 2021). NHC Tech. Rep. AL082021, 42 pp., https://www.nhc.noaa.gov/data/tcr/AL082021_Henri.pdf.

Rios-Berrios, R., and R. Torn, 2017: Climatological analysis of tropical cyclone intensity changes under moderate vertical wind shear. *Mon. Wea. Rev.*, **145**, 1717–1738, https://doi.org/10.1175/MWR-D-16-0350.1.

Stettner, D., C. S. Velden, R. Rabin, S. Wanzong, J. Daniels, and W. Bresky, 2019: Development of enhanced vortex-scale atmospheric motion vectors for hurricane applications. *Remote Sens.*, **11**, 1981, https://doi.org/10.3390/rs11171981.

Takemura, K., and H. Mukougawa, 2021: Tropical cyclogenesis triggered by Rossby wave breaking over the western North Pacific. *SOLA*, **17**, 164–169, https://doi.org/10.2151/sola.2021-029.

Zhang, G., Z. Wang, T. J. Dunkerton, M. S. Peng, and G. Magnusdottir, 2016: Extratropical impacts on Atlantic tropical cyclone activity. *J. Atmos. Sci.*, **73**, 1401–1418, https://doi.org/10.1175/JAS-D-15-0154.1.

——, ——, M. S. Peng, and G. Magnusdottir, 2017: Characteristics and impacts of extratropical Rossby wave breaking during the Atlantic hurricane season. *J. Climate*, **30**, 2363–2379, https://doi.org/10.1175/JCLI-D-16-0425.1.